SWITCHING DEFORMATION MODE AND MECHANISMS DURING SUBDUCTION OF CONTINENTAL CRUST:
A CASE STUDY FROM ALPINE CORSICA

Giancarlo Molli [a], Luca Menegon [b], Alessandro Malasoma [c]

a Dipartimento di Scienze della Terra, Università di Pisa, Via S. Maria, 53, Pisa 56126, Italy

b School of Geography, Earth and Environmental Sciences, Plymouth University, Plymouth, UK

c TLS Lab and Geoservices, Via Vecchia Fiorentina, 10, 56023 Cascina, Pisa Italy

Correspondence to: Giancarlo Molli (giancarlo.molli@unipi.it)

Abstract. The switching in deformation mode (from distributed to localized) and mechanisms (viscous versus frictional) represent a relevant issue in the frame of crustal deformation, being also connected with the concept of the brittle-"ductile" transition and seismogenesis. In subduction environment, switching in deformation mode and mechanisms may be inferred along the subduction interface, in a transition zone between the highly coupled (seismogenic zone) and decoupled deeper aseismic domain (stable slip). On the other hand, the role of brittle precursors in nucleating crystal-plastic shear zones has received more and more consideration being now recognized as fundamental in the localization of deformation and shear zone development, thus representing a case in which switching deformation mode and mechanisms interact and relate to each other. This contribution analyzes an example of a crystal plastic shear zone localized by brittle precursor formed within a host granitic-protomylonite during deformation in subduction-related environment. The studied structures, possibly formed by transient instability associated with fluctuations of pore fluid pressure and episodic strain rate variations may be considered as a small scale example of fault behaviour associated with a cycle of interseismic creep and coseismic rupture or a new analogue for episodic tremors and slow slip structures. Our case-study represents, therefore, a fossil example of association of fault structures related with stick-slip strain accomodation during subduction of continental crust.

1. Introduction

The study of deformation fabric of fault rocks has been the base to develop a general model for crustal scale fault zones (Sibson, 1977; Sibson, 1983; Scholz, 1988; Scholtz, 2002; Handy et al., 2007; Cooper et al. 2010; Platt and Behr, 2011). In this model, the increasing PT conditions determine the transition from a seismogenic frictional regime, dominated by pressure-sensitive deformation and involving cataclasis and frictional sliding, to a viscous regime (Rutter, 1986; Schimd and Handy, 1991; Handy and Brun, 2004), where dominantly aseismic, mainly crystal-plastic and continuous shearing is localized within mylonitic shear zones. In quartzo-feldspathic rocks, this transition is primarily determined by temperature-related quartz response to change in deviatoric stress, with dislocation creep becoming the principal deformation mechanism at T>270 °C (Stipp et al., 2002 and references).

Rock deformation experiments (Rutter, 1986; Shimamoto and Logan 1986; Bos and Spiers 2002; Scholz 2002) have shown that the shear strength of simulated faults at the brittle-viscous transition may depend on normal stress (as ~~by~~ faulting dominated by cataclastic mechanisms) although strain is achieved through crystal plasticity and/or solution transfer. These results support the ~~hypothesis~~ that some mylonitic shear zones are produced by coupled frictional and viscous mechanisms under semi-brittle conditions (Shimamoto and Logan, 1986; Shimamoto, 1989; Chester, 1989; Scholz, 2002; Pec et al., 2012 and references). Studies on semi-brittle behaviour leave several open questions regarding natural fault zones including micromechanisms controlling bulk-rock deformation, the degree of interdependence of active deformation mechanisms, their cyclicity and the associated bulk rock style of deformation (Sibson, 1980; White and White, 1983; Takagi et al., 2000; Handy and Brun, 2004; Pec et al., 2012). Complex transitional behaviour involving mixed continuous and discontinuous, distributed vs. localized, and cyclic switching in deformation mechanisms over large variations in strain rates is inferred at the transition between frictional and viscous domains, a zone which includes the typical hypocentres and rupture depths for large earthquakes in continental crust (Sibson, 1983; Kohlstedt et al., 1995; Scholz, 2002; Handy and Brun, 2004).

In ~~convergent~~ subduction settings, ~~similarly,~~ the transition zone, located between 10 and 35 km depth depending on slab dip and thermal structure (i.e., between temperatures of 150 °C and 350–450 °C), along subduction interfaces is recognized as the site of megathrust earthquake nucleation and concentrated postseismic afterslip, as well as the focus site of episodic tremor and slow slip events (Hacker et al., 2003; Vannucchi et al., 2008; Meneghini et al., 2010; Angiboust et al., 2012; Andersen et al., 2014; Hayman and Lavier, 2014; Fagereng et al., 2014; Angiboust et al., 2015).

The feedback between brittle and viscous deformation modes is relevant also for the mechanisms of shear zone nucleation, ~~so~~ that fracturing has been proposed to be ~~even~~ a pre-requisite for the initiation of ductile shear zones in the lithosphere (Handy and Stünitz, 2002; Pennacchioni and Mancktelow,

75   2007; Fusseis and Handy, 2008, among others). Shear zones and style of strain accommodation in terms

76   of distributed vs. localized deformation in granitoids have been described by different authors (Ramsay

77   and Graham, 1970; Burg and Laurent 1978; Simpson, 1983; Gapais et al. 1987; Goncalves et al. 2016

78   and references therein). In this context, the role of brittle precursors in nucleating crystal-plastic shear

79   zones has received ~~more and more~~ consideration ~~being now recognized as having~~ a fundamental role in

80   ~~the~~ localization ~~process~~ (Segall and Simpson, 1986; Mancktelow and Pennacchioni, 2005;

81   Pennacchioni, 2005; Pennacchioni and Mancktelow, 2007; Menegon and Pennacchioni, 2010;

82   Pennacchioni and Zucchi 2012, among others).

83   However these works mostly deal with brittle precursors consisting of inherited structures such as

84   ~~discontinuities already existing at the beginning of deformation,~~ as ~~the cases of~~ cooling joints,

85   cataclasites and veins (e.g. Guermani and Pennacchioni, 1998; Pennacchioni and Mancktelow 2007)

86   and most of them consider deformation at shallow to intermediate crustal depths (Fusseis and Handy,

87   2008; Mazzoli et al., 2009; Molli et al., 2011) although case studies framed under conditions of upper

88   amphibolite to granulite facies (White, 1996; Pennacchioni and Cesare, 1997; Kisters et al., 2000;

89   Pittarello et al., 2013; Altenberger et al., 2013) and eclogite facies (Austrheim and Boundy, 1994;

90   Austrheim, 2013 and references therein) ~~were~~ also investigated.

91   The case of deformation of crustal units and granitoids during subduction has been only recently

92   analysed in terms of rock records of paleo-seismic cycle and/or slow-slip phenomena (Angiboust et al.,

93   2015). A well-documented study from the Dent Blanche Thrust in the Western Alps is framed in the

94   hangingwall of an ancient subduction interface zone (Angiboust et al., 2014; 2015). ~~On the contrary,~~

95   our contribution analyses a microscale example of brittle precursor ~~of~~ a crystal plastic shear zone

96   derived from the footwall of a subduction interface ~~in ambient~~ blueschist-facies conditions thus

97   representing ~~a still not yet or less documented~~ case study (Molli et al., 2005; Molli 2007).

98   By virtue of their deep origin, the analysed structures are ideally suited to contribute to the ongoing

99   discussion on the deformation style and mechanisms associated with the broad spectrum of fault-slip

100   behaviour (from seismic slip to stable aseismic creep, to episodic slow slip events and non-volcanic

101   tremors) recorded by seismic and geodetic observations at active plate boundaries (e.g. Peng and

102   Gomberg 2010; Beroza and Ide, 2011, and references therein). Slow slip events (i.e. fault slip events

103   with slip rates in between coseismic slip and aseismic creep, and generating equivalent seismic

104   moments similar to large earthquakes) in subduction zones have been recorded in a depth interval that

105   experiences temperatures between 250 and 650° C and pressures between 0.6 and 1.2 GPa (Beroza and

106   Ide, 2011), typically in areas of high Vp/Vs ratios suggestive of local high fluid pressures. This locates

107   slow slip events at the lower end of the seismogenic zone, at metamorphic conditions where the

108   rheology is expected to be viscous or at the frictional-viscous transition. Accordingly, recent studies of

109 shear zones exhumed from similar conditions along the subduction interface have suggested that

110 coupled fracture and viscous flow, possibly associated with fluctuations in fluid pressure, can ~~originate~~

111 tremors and slow slips (e.g. Fagereng et al., 2014; Hayman and Lavier, 2014; Angiboust et al., 2015;

112 Malatesta et al., 2017). Here we show that the HP brittle-viscous transition preserved in the Popolasca

113 granitoids can also be explained with transient high fluid pressures triggering brittle deformation in an

114 otherwise viscous regime, and discuss the related implications for fault-slip behaviours in subduction

115 zones.

116

2. Regional background and Geological Setting of studied sample

118 In Alpine-type orogens the study of meso- and microstructural record of exhumed subduction related

119 thrust zones and its interpretation in terms of subduction zone rheology and seismicity have received

120 increasing attention ~~since the end of '90~~ (Stöckhert et al.,1999; Kuster and Stöckhert, 1999). This

121 subject has been developed in ~~particular in the~~ Alpine Corsica (Austrheim and Andersen, 2004;

122 Andersen and Austrheim, 2006; Healy et al., 2009; Andersen et al., 2014; Deseta et al., 2014a,b; Magott

123 et al., 2016a,b) ~~in~~ oceanic units ~~made up of~~ peridotite, serpentinite, gabbro, basalt, calcareous and

124 siliceous schist and marble exposed as remnants ~~of the lithosphere~~ of the Jurassic Piemonte- Liguria

125 oceanic basin and its pelagic sedimentary cover (Mattauer et al., 1981; Bezert and Caby, 1988; Jolivet

126 et al., 1990; Molli, 2008; Vitale Brovarone et al., 2013).

127 These widespread occurrences ~~and preservations~~ of relicts ~~of~~ seismogenic ~~exhumed~~ structures are

128 mainly related to the peculiar geologic history of Alpine Corsica, connected with the development of

129 the Alps/Apennine orogenic system (Molli and Malavieille, 2011; Guyedan et al., 2017; Beaudoin et al.,

130 in press) ~~with the lacks of~~ the continent-continent "hard collision"- related structures and thermal

131 reworking observable in the Alps (e.g. Polino et al., 1995; Schmid et al., 1997; Berger and Busquet,

132 2008; Butler, 2013; Rosenberg and Kissling, 2013; Carminati and Doglioni, 2014) ~~and a better~~

133 ~~preservation of~~ the early stages of subduction-related structures and fabrics.

134 Corsica, therefore, represents a ~~suitable~~ natural laboratory for the investigation of the subduction-related

135 processes in oceanic and continental crust as firstly suggested by Mattauer et al. (1981) and Gibson and

136 Horak (1984).

137 ~~In Corsica, continental~~ derived units, ~~i.e. units~~ ~~derived~~ from the footwall of ancient subduction interface

138 zone, can be observed in three different structural positions (Fig.1), each of them corresponding to a

139 different peak metamorphism (Tribuzio and Giacomini, 2004; Molli, 2008; Vitale Brovarone et al.,

140 2013):

141 the innermost slices (Serra di Pigno/Farinole units) interleaved with oceanic units show eclogite peak

142 conditions at 1,5/1,8 GPa; 500 ± 50 °C;

143 - the intermediate ones (e.g. the Tenda and Centuri units) are instead characterized by Upper Blueschist

144 facies peak conditions at 0,9/1,1 GPa; 450± 50 °C;

145 - the most external (e.g. Corte/Popolasca units) show high pressure greenschist and/or blueschist facies

146 peak assemblages developed at T =325/370°C, P = 0.75/0.85 GPa (Malasoma et al., 2006; Di Rosa et

147 al., 2016).

148 These occurrences document the progressive underthrusting at different depths and their in-sequence

149 contractional exhumation within an [] e-age east-dipping subduction system (Mattauer et al., 1981;

150 Bezert and Caby, 1988; Jolivet et al., 1990; Garfagnoli et al., 2009; Molli and Malavieille, 2011; Maggi

151 et al., 2012; Di Rosa et al., 2016; Guyedan et al., 2017).

152 The studied samples come from the external continental units (Molli, 2008; Molli and Malavieille,

153 2011; Vitale Brovarone et al., 2013) of Alpine Corsica and in more detail from the Popolasca Unit

154 (Bezert and Caby, 1988; Malasoma et al., 2006; Di Rosa et al., 2016). This unit is characterized by a

155 pre-Mesozoic basement mainly formed by granitoids, a Permo-Mesozoic metasedimentary sequence

156 and an Early-Eocene flysch (Fig. 1).

157 Blueschist assemblages in the unit have been described by regional studies (Bezert and Caby, 1988;

158 Malasoma et al., 2006; Molli, 2008; Di Rosa et al., 2016) and can be observed in all suitable rock-types:

159 in metapelites from cover rocks, in metabasic dykes and some of the granitoid suites from the basement.

160 Peak metamorphism has been constrained at 250/350°C, 0.4/0.55 GPa (Bezert and Caby, 1988) or more

161 recently better defined at 325/370 °C and 0.75/0.85 GPa (Malasoma et al., 2006; Di Rosa et al., 2016).

162 The prograde to peak pressure assemblage has been recently dated in the range of 45-36 Ma by Di

163 Vincenzo et al., (2016).

164 The contributions of Malasoma et al., (2006), Di Rosa et al., (2016) analysed the cartographic to

165 mesoscopic-scale structural geometries of deformation in the area of the studied sample.

166 Superimposed foliations and fold structures are typical of the metasedimentary cover, with blueschist

167 assemblages as relict fabrics. On the contrary, in basement rocks a main phase continuous foliation can

168 be observed wrapping around undeformed granitoids. The main foliation is either associated with

169 blueschist or greenschist facies assemblages (Malasoma et al., 2005; Di Rosa et al., 2016; Di Vincenzo

170 et al., 2016). Anastomosed network of fault zones associated with subgreenschist facies assemblages

171 overprints all previous structures and may be related to the activity of a major N/S trending transcurrent

172 fault zone (Central Corsica Fault Zone) reworked by normal kinematics active during Oligocene-

173 Miocene in the frame of rototranslation of Corsica-Sardinia microblock and upper-plate extension

174 associated with Apenninic subduction (Faccenna et al., 2004; Molli, 2008; Molli and Malavieille, 2011;

175 Carminati and Doglioni, 2014; Guyedan et al, 2017).

176

177

3. Geometry of deformation and microstructures

179 The analysed sample (Fig.2) is a deformed granitoid ~~of calcalcaline suite~~ (K-feldspar, plagioclase,

180 quartz, biotite) ~~well known in the~~ Hercynian Corsica (Rossi et al., 2001). It shows a continuous

181 foliation (Fig.2,3a,b) mainly defined by the shape preferred orientation of quartz, feldspars and biotite

182 grains.

183 Shape anisotropy of quartz in the host protomylonite shows an aspect ratio around 0,37 (mean X/Z of

184 2,7) which indicates a shear strain γ of c.1 assuming deformation in simple shear.

185 Quartz shows ~~typical~~ features of low temperature plasticity (Tullis et al., 2000; Stipp et al., 2002;

186 Vernooij et al., 2006; Trepmann et al., 2007; Derez et al., 2015; Kjøll et al., 2015) (Fig 3), such as

187 undulatory extinction, localized extinction bands (LEBs, following the terminology of Derez et al.,

188 2015), typically forming conjugate sets, and up to 100 µm thick intracrystalline bands of recrystallized

189 grains (5-10 µm in size). Bands of recrystallized grains occur parallel to the main foliation as well as in

190 conjugate sets intersecting at ca. 90° and parallel to the conjugate sets of LEBs.

191 Feldspars show local evidence of grain size reduction by microcraking and microfaulting (Fig.3)

192 associated with K-feldspar breakdown to albite (by bulging recrystallization) (Fig.3), stilpnomelane and

193 phengite. Thin needles of Na-amphibole (Fig.4) attest the development of this fabric in HP/LT

194 conditions as described below.

195

196 The main foliation is cross-cut at high angle by a millimetre-thick localized zone of deformation

197 (Fig.2,5). This shows a sharp boundary, truncating flattened quartz and feldspar grains; a feature

198 suggesting its development as unstable fracture (Schmid and Handy, 1991; Passchier and Trouw, 2011).

199 Three compositionally controlled domains can be recognized within the thin localized shear zone

200 (Fig.2,5):

201 Domain 1 is feldspar-dominated and shows microstructural features typical of a cataclasite (Fig.5a,c).

202 Feldspar clasts (and quartz grains) reveal both displacive intragranular fractures and intergranular

203 "stable" cracks (Atkinson, 1982; Schmid and Handy, 1991).

204 Domain 2 is "phyllosilicate"-dominated (stilpnomelane and phengite) and shows microstructural

205 features of a foliated-cataclasite/phyllonite (Fig.5a,b). Asymmetric porphyroclasts and shear band

206 systems characterize the phyllosilicate-rich parts of the shear zone.

207 Domain 3 is a quartz-albite rich domain showing microstructural features typical of an ultramylonite.

208 This is characterized by very fine recrystallized albite and quartz grains (5-10 µm in size) (Fig.5a,b;

209 Fig.6) with strong crystallographic preferred orientation (see below). Quartz porphyroclast shows a

210 mean aspect ratio around 0,09 (mean X/Z of 11) which corresponds to a calculated shear strain γ of c. 3

211 At this shear strain the corresponding angle between the foliation and the shear zone boundary in simple

212 shear is around 15 ° which agrees with the mean orientation of the quartz porphyroclasts shape

213 preferred orientation defining the ultramylonitic foliation (Fig.6a,b,c) Syn to post-kinematic Na-

214 amphibole (Fig.6a) documents shearing in HP/LT metamorphic conditions, as illustrated ~~here~~ below.

215

216 **4. Mineral chemistry and estimate of metamoprphic Pressure-Temperature (P-T) conditions**

217 Chemical analyses of coexisting minerals within the metamorphic assemblage (Tab.1) were obtained

218 using a JEOL JXA-8600 electron microprobe, equipped with four wavelength-dispersive spectrometers,

219 at the CNR - Istituto di Geoscienze e Georisorse, Firenze, Italy. Running conditions were 15 kV

220 accelerating voltage and 10 nA beam current on a Faraday cage. Counting time for the determined

221 elements ranged from 10 to 60 s at both peak and background. The Bence and Albee (1968) method

222 was employed for the correction of all data. A number of synthetic and mineral standards were used for

223 instrumental calibration.

224 **Amphibole.** Structural formulae were calculated assuming 23 oxygens, and the classification of Leake

225 et al. (1997) was adopted. Site assignment and ferric iron contents were calculated using the scheme

226 proposed by Schumacher in Leake et al. (1997). Because of the small sizes of the crystals (widths

227 *c*.10μm), it was not possible to make compositional traverses across individual crystals to detect

228 intracrystalline variations in chemical composition, such as core-to-rim zonation. Thus, each analysis

229 reported in Table 1 ~~represents~~ a different crystal. In the studied sample the Na-amphiboles are mostly

230 riebeckite (Tab.1 and Fig. 4b) with low $Mg/(Mg+Fe^{2+})$ ratio (0.13-0.21) and are characterized by Si

231 contents close to the maximum of 8.0 apfu.

232 **Other minerals.** ~~All analysed albites, of which structural formulae~~ were calculated assuming 8

233 oxygens, have composition close to the pure end-member. Stilpnomelane structural formulae were

234 calculated assuming 24 oxygens and all Fe as divalent (Fe^{2+}). Stilpnomelanes have Fe amounts ranging

235 from 1.86 to 2.91 apfu and Mg amounts ranging from 0.24 to 0.58 apfu. For K-feldspar and biotite

236 porphyroclasts, structural formulae were calculated assuming ~~respectively~~ 8 and 22 oxygens. The

237 analysed K-feldspars have composition close to the orthoclase pure end-member, with minor amounts

238 of Na.

239

240 The peak metamorphic mineral assemblage is ~~characterised~~ by Na-amphibole + phengite + quartz +

241 albite + stilpnomelane. Na-amphibole is a typical mineral related to the blueschist facies and is

242 indicative of HP/LT gradient metamorphism (e.g. Evans 1990; Schiffman & Day 1999 and references).

243 The minimum temperature (T) and pressure (P) conditions of this mineral assemblage can be estimated

244 using the reaction curves proposed by Schiffman & Day (1999) for the appearance of Na-amphibole

245   (stability field of the blueschist facies); meanwhile the maximum temperature (T) conditions were

246   constrained by the presence of stilpnomelane, as shown by the equilibrium: Stp+Phe=Bt+Chl+Qtz+W

247   (Massonne & Szpurka, 1997). Summing up all the available thermobarometric information, the

248   metamorphic conditions can be estimated as temperature (T) around 320±50 °C and pressure (P) > of

249   0.70 GPa (Fig.4c); consistent with those described by Malasoma *et al.* (2006) in metagranitic rocks

250   from the area of our studied sample.

251

252

253

254   **5. EBSD data**

255   EBSD analysis of quartz was conducted with a Jeol 7001 FEG-SEM equipped with a NordlysMax

256   EBSD detector (Oxford Instruments) at the Plymouth University Electron Microscopy Centre. Working

257   conditions during acquisition of the EBSD patterns were 20 kV, 70° sample tilt and high vacuum. Thin

258   sections were chemically polished with colloidal silica and carbon-coated before the analysis. EBSD

259   patterns were acquired on rectangular grids with step size of 1 μm and 2 μm. EBSD patterns were

260   acquired and indexed with the AZtec software and processed with Channel 5 software (Oxford

261   Instruments). Raw EBSD data were processed to reduce data noise following the procedure tested by

262   Prior et al. (2002) and Bestmann and Prior (2003). EBSD results are shown ~~in form of~~ Inverse Pole

263   Figure map, pole figures ~~(equal angle, lower hemisphere)~~ of crystallographic axes and planes (<0001>

264   c-axis, <11-20> a-axis, {10-10} prism {m}, {10-11} positive rhomb {r}, {01-11} negative rhomb {z}),

265   misorientation pofiles and plots of misorientation axis in sample coordinates.

266

267   **5.1 Quartz in the host rock**

268   We analysed a monocrystalline quartz ribbon elongated parallel to the host-rock foliation and sharply

269   cut by the thin localized shear zone. The quartz ribbon contains two nearly orthogonal sets of

270   intracrystalline shear bands of recrystallized grains (Fig. 7a); one set is oriented at high angle (90° ± 20,

271   *set 1*) and one at low angle (≤ 20°, *set 2*) to the host rock foliation (vertical in Fig. 7a). The average

272   grain size of the recrystallized grains is 5±2 μm. The ribbon contains ~~also fine localized~~ extinction

273   bands ~~(~~up to 20 μm thick~~)~~ (LEBs: Derez et al., 2015) subparallel to the bands of recrystallized grains.

274   Low-angle boundaries are ubiquitous in the ribbon; on EBSD maps they are typically straight, poorly

275   connected, and subparallel to the bands of recrystallized grains (Fig. 7b). Some low-angle boundaries

276   are connected to form subgrains of approximately the same size of the recrystallized grains. Subgrains

277   occur with a higher frequency at the intersection between two sets of recrystallized bands, and in

278   regions sandwiched between closely spaced (≤ 100 μm) subparallel bands of recrystallized grains (Fig.

279 7b).

280 The c-axis of the ribbon is oriented near the pole to the host-rock foliation, i.e. in a position suitably

281 oriented for the activation of the basal <a> slip system of quartz (Fig. 7c). The c-axis orientation of the

282 recrystallized grains in the intracrystalline bands is mostly spread out along the periphery of the pole

283 figure, although some scattered grains have their c-axis in intermediate positions between the X and Y

284 directions of the pole figures (Fig. 7d). Such an orientation suggests that the recrystallized grains have

285 experienced a rotation around the Y-direction of finite strain (i.e. centre of the pole figure) from the

286 host-grain orientation (e.g. Van Daalen et al., 1999; Menegon et al., 2011).

287 This is confirmed by the boundary trace analysis (Prior et al., 2002; Menegon et al., 2010) of the two

288 main sets of straight low-angle boundaries defining localized extinction bands (parallel to bands of

289 recrystallized grains), one running ENE-WSW (*subset1*) and one running ca. N-S (*subset 2*) in Fig. 7b.

290 The dispersion paths of crystallographic directions on the pole figures of subset 1 (Fig. 7e) identifies

291 {m} as the rotation axis, which lies very close to the centre of the pole figure. The pole to the prismatic

292 plane {m} is the rotation axis associated with the basal <a> and with the {a} <c> slip system in quartz

293 (e.g. Neumann, 2000), and, accordingly, subset 1 can be interpreted as a tilt boundary plane produced

294 by the activity of the slip system basal <a> (Fig. 7e) and containing the boundary trace of subset 1 and

295 the rotation axis.

296 Subset 2 has a similar dispersion path as subset 1, with {m} as the identified rotation axis. However, in

297 this case the boundary trace analysis is not consistent with a tilt boundary produced by the activity of

298 the slip system basal <a>, but could indicate the activity of the {a} <c> slip system (Fig. 7f). However,

299 activity of c-slip in quartz typically requires temperature in excess of 600° C (Kruhl, 1996; Zibra et al.,

300 2010) and, therefore, appears unlikely in our samples. Moreover, misorientation profiles across low-

301 angle boundaries with a subset 2 orientation show abrupt misorientation jumps of up to 6° (profiles 2

302 and 3 in Figs. 7b and 7g), as opposed to a gradual accumulation of misorientation towards low-angle

303 boundaries with a subset 1 orientation (profile 1 in Figs. 7b and 7g). Thus, the low-angle boundaries

304 with a subset 2 orientation could represent microcracks subparallel to the basal planes (e.g. Kjøll et al.,

305 2015) that localized rigid body rotation of fragments around the Y-direction (e.g. Trepmann et al., 2007;

306 Menegon et al., 2013). The rotation around Y of (1) the crystallographic directions of the host grain and

307 (2) the recrystallized grains (in this case for large misorientation > 10°) is confirmed by the plots of the

308 misorientation axis in sample coordinates (Fig. 2).

309

310 **5.2 Quartz in the localized shear zone**

311 We analysed polycrystalline ribbons of recrystallized grains from domain 3 of the localized shear zone

312 (Fig. 8a). The c-axis orientation of the recrystallized grains defines an inclined type-I crossed girdle

313   synthetically oriented with respect to the bulk shear sense of the shear zone (Fig. 8b). The c-axes are

314   preferentially clustered near the pole to the shear zone boundary, i.e. in an orientation suitably oriented

315   for the activity of the basal <a> slip system. ~~The average grain size of the recrystallized grains in~~

316   ~~domain 3 is 6±2 μm.~~

317

318   **6. Ultramylonite: Paleopiezometry, flow stress and strain rate**

319   The microstructure and the crystallographic preferred orientation of quartz indicate that quartz in the

320   protomylonite and ultramylonite deformed by dislocation creep (concomitant with microcracking in the

321   protomylonite) and recrystallized to a fine-grained aggregate. Thus, the rheology and the flow stress in

322   the ultramylonite can be evaluated extrapolating experimentally calibrated flow laws of quartz to the

323   deformation conditions.

324   The rheology of quartz deforming by dislocation creep is generally described in terms of a power-

325   law equation:

326        $$\dot{\varepsilon} = A f_{H_2O}^m e^{(-Q/RT)} \sigma^n$$

     (1)

327   Where $\dot{\varepsilon}$ is the strain rate, f_{H2O} is the water fugacity (raised to the power of m), Q is the activation

328   energy, R is the universal gas constant, T is the temperature, σ is the differential stress, and n is the

329   stress exponent. We used the ~~theoretical~~ dislocation creep flow law ~~of~~ Hirth et al. (2001), which ~~has~~

330   ~~derived~~ a linear dependence of strain rate on the water fugacity (m=1) and a stress exponent of 4. A

331   water fugacity of 172 MPa ~~is calculated from the water fugacity coefficient reported in Tödheide (1972)~~

332   at T=350° C, P=0.8 GPa.

333   The paleostress (assuming steady-state flow at time of viscous deformation) can be determined by

334   recrystallized quartz grain size paleopiezometer (e.g. Stipp & Tullis, 2003), which ~~have~~ been calibrated

335   in the form: Δσ = B D $^{-x}$, where Δσ is the steady state differential stress (σ1 ~~- σ3~~), D is the recrystallized

336   grain size and B and X are empirical constants. Using the recrystallized grain size piezometer of quartz

337   calibrated by Stipp and Tullis (2003), a recrystallized grain size of 5-10 μm indicates differential stress

338   in the range of 110-190 MPa. ~~Extrapolation~~ of the flow law of Hirth et al. (2001) yields a strain rate in

339   the range of ~~7.6~~* 10^{-13} – ~~6.2~~* 10^{-12} sec^{-1} in the ultramylonite at the estimated deformation temperature

340   of 350° C.

341

342   **7. Discussion and conclusion**

343

344   **7.1 Viscous-brittle-viscous deformation under HP/LT conditions**

345 The analysed example documents a switch in deformation mode and mechanisms within an HP/LT fault

346 zone. ~~On the base of~~ overprinting relationships and microstructural ~~features~~ the following deformation

347 sequence ~~may be suggested:~~ stage (1), ~~associated with a~~ distributed deformation and development of a

348 protomylonitic foliation in the granitoid by quartz low temperature plasticity, microfracturing, and

349 albite neo-crystallization from K-feldspar porphyroclasts (Fitzgerald and Stunitz, 1993), has been

350 followed by stage (2), in which localized deformation by brittle fracturing formed a millimeter-thick

351 cataclasite, which acted as a precursor for (3) localization of viscous deformation and ultramylonite

352 development. The synkinematic and postkinematic growth of Na-amphibole in the host rock foliation

353 and in localized ultramylonite indicates that the entire deformation sequence occurred at HP/LT

354 conditions (ca. 350°C at ≥ 0.7GPa), corresponding to a ==depth of 23-30 km== in the ==sub==duction channel.

355 The estimated P, T conditions are consistent with ==low-T plasticity regime in quartz (==Stipp et al., 2002;

356 Derez et al., 2015 and refs therein). Accordingly, the deformation microstructures of quartz produced

357 during stage (1) in the host rock appear to be the product of the competition between dislocation activity

358 and fracturing. Localized extinction bands at high angle to the host rock foliation (subset 1 in Fig. 7b)

359 are consistent with the activity of the basal <a> slip system, whereas localized extinction bands

360 subparallel to the host-rock foliation (subset 2 in Fig. 7b) are interpreted as fractures subparallel to the

361 basal plane, as previously observed by Kjøll et al. (2015). Some localized extinction bands (especially

362 those with a subset 2 orientation, see Fig. 7b) contain isolated small new grains that are considerably

363 smaller than the average grain size in the recrystallized bands, and that are only slightly misoriented

364 with respect to the host grain. Moreover, the high-angle boundaries in such localized extinction bands

365 are not always fully connected to define entire new grains. Together with the abrupt misorientation

366 jumps (Fig. 7g), these observations further suggest that localized extinction bands with a subset 2

367 orientation represent fractured domains in which the fragments have rotated passively and sealed

368 together as proposed by e.g. Derez et al. (2015).

369 ~~Despite~~ the local fracturing of the host grain, deformation of the recrystallized grains in the conjugate

370 intracrystalline bands involved dislocation activity, as indicated by the cluster of misorientation axis

371 around the prism {m} for low misorientations (compare Fig. 7h with 7d). This is consistent with the

372 local activity of the basal <a> slip system in the recrystallized bands, as also indicated by the CPO of

373 the recrystallized grains in the bands at high angle to the host rock foliation (Fig. 7d).

374 The type-I crossed girdle c-axis CPO of quartz in the ultramylonite suggests the concomitant activity of

375 basal <a>, rhomb <a> and prims <a> slip systems in the recrystallized ribbons (Fig. 8). The grain size

376 of recrystallized quartz in the ultramylonites is in the same range (5-10 μm) as in the intracrystalline

377 bands in the host rock. This suggests that 5-10 μm represents the equilibrium grain size ~~with~~ the flow

378 stress (estimated in the range of 110-190 MPa with recrystallized grain size piezometry) during viscous

379   deformation before and after the transient brittle event of stage (2).

380   During stage (2) the development of cataclasite and related dilatancy resulted in an increase of

381   permeability and thus facilitated fluid access and fluid mobility in the shear zone. This enhanced

382   mineral transformations as testified by modal enrichment of stilpnomelane (by biotite breakdown) and

383   Na-amphibole in the ultramylonite.

384   Therefore, the observed structures witness a change in deformation style (from distributed to localized

385   strain in brittle precursor), and a switch in the dominant deformation mechanism (from low T plasticity

386   in the host rock to cataclasis and back to crystal plasticity in the ultramylonite), which occurred at the

387   footwall of subduction interface at temperature conditions typical of the brittle/viscous transition in

388   quartz/feldspathic rocks.

389   Finally, the transition from stage (2) and stage (3) is consistent with the general observation that

390   nucleation of localized ductile shear zones ~~requires~~ the presence of a planar compositional or structural

391   precursor (e.g. Pennacchioni and Zucchi, 2012, and references therein). The example from the

392   Popolasca granite demonstrates that (i) nucleation on brittle precursors also occurs under HP/LT

393   conditions in the subduction channel, and (ii) the brittle precursors are not necessarily inherited from an

394   earlier deformation event, but can be the manifestation of switches in deformation mode in the footwall

395   of the subduction interface.

396

397   **7.2 Significance of the switch in deformation mode and implications for fault-slip behaviours in**

398   **subduction zones**

399   We interpreted the inferred deformation sequence and structures as the result of transient instabilities

400   (Sibson, 1980; White, 1996; Handy and Brun, 2004) possibly representative of mixed fault-slip

401   behaviours at seismogenic depth in the subduction channel. We have estimated the conditions resulting

402   in the transient brittle event during stage (2) under the following assumptions and approximations:

403   1. The coefficient of internal friction, μ_i, is generally between 0.5 and 1.0 in intact rocks (Sibson,

404   1985). We considered $\mu_i = 0.6$ in the failure envelope for the intact Popolasca granitoid.

405   2. We used a cohesive strength of 35 MPa as representative for granitoids (Amitrano and

406   Schmittbuhl, 2002), with a resulting tensile strength of 17.5 MPa.

407   3. We assumed and Andersonian stress field and a thrust regime. The effective vertical stress σ'_v

408   corresponds to the effective minimum principal stress $\sigma'_3 = \sigma_3 - P_f$, where P_f is the pore fluid

409   pressure. We considered a hydrostatic pore pressure ($\lambda = 0.4$, $P_f = 320$ MPa for $\sigma_3 = 800$ MPa)

410   during the formation of the gneissic foliation in the host rock.

411   4. We assumed a differential stress of 110-190 MPa during viscous flow of the granitoid prior to

412   brittle failure at σ'_v = 480 MPa, as derived from the recrystallized grain size piezometry in the

413   protomylonite.

414   The results of our analysis are shown in Fig. 9a. For brittle failure, it is necessary to invoke high

415   differential stresses (of the order of 1.1 GPa assuming a hydrostatic pore fluid pressure), or higher fluid

416   pressure (Fig. 9a). Differential stresses in excess of 1 GPa have been associated with intermediate depth

417   (50-300 km) earthquakes in the subduction channel (e.g. John et al., 2009), and are expected to result in

418   extensive development of pseudotachylytes in granitoid rocks (e.g. Austrheim 2013 and references

419   therein), which, on the contrary, have not been observed in the sample studied here.

420   For the differential stress range and the vertical stress considered here, brittle failure requires

421   (sub)lithostathic fluid pressure (0.96 < λ < 1, Fig. 9). The strength envelope plotted for pore fluid

422   pressure between 0.98 and 0.94 and for a strain rate of 10^{-12} s^{-1} (Fig. 9b) suggests that viscous

423   deformation at the estimated depth range (23-30 km) is only possible for pore fluid pressure $\leq$ 0.94,

424   otherwise brittle deformation is expected to occur. Thus, under the assumptions listed above, ~~our~~

425   ~~analysis indicates that~~ local fluctuations in pore fluid pressure can explain the cyclic viscous-brittle-

426   viscous deformation switch. However, despite the synkinematic growth of hydrous minerals in the

427   cataclasite and the high pore fluid pressure required at failure, there is no evidence of macroscopic

428   veining or hybrid fractures in the samples. Our analysis is consistent with this observation, in that

429   failure occurs entirely in the shear fractures field and not in the (hybrid) shear extension fractures field

430   (Fig. 9a).

431   Drawing from the results shown in Figs. 9a,b and using concept and inferences coming from modern

432   studies of convergent subduction system (e.g. Ozowa et al., 2002; Fu and Freymuller, 2013; Bedford et

433   al., 2013) ~~we may suggest~~ the following deformation path (Fig.10) ~~for the structural features of our~~

434   ~~analysed sample~~. A first stage of distributed deformation (stage 1) may be associated with ~~large~~ scale

435   anastomosed shear zone development and aseismic creep, then, following Angiboust et al. (2015), two

436   possible deformation scenario and slip patterns may be envisaged: (a) propagation at seismic rate of

437   microrupture followed by afterslip or (b) slow slip phenomena in an aseismically creeping crust. In the

438   first case transient strain rate increase associated with brittle fracturing would represent the deep

439   response of the transition zone to a specific stage of the seismic cycle taking place higher up along the

440   seismogenic portion of the subduction interface (Fig.10c, scenario 1) or in less deformed domains

441   acting as local stress raisers nearby (Fig.10c, scenario 2). Cataclastic deformation would then correlate

442   with coseismic to postseismic deformation higher up along the interface. In that case, the mylonitization

443   of the brittle precursor would be the record of subsequent interseismic deformation at lower strain rates,

444   taking place in the time frame between two earthquakes.

445   In the second case (Fig.10d), the transient highs in strain rates related to brittle fracturing and cataclasis

446 could be the ~~field evidence of deformation associated with~~ slow slip events (SSEs) or other transient

447 slips, generally localized along the subduction interface at this depth range itself (e.g., Shelly et al.,

448 2006; Fagereng et al., 2014). We are aware that the mechanism(s) of SSEs initiation are still poorly

449 understood, and that stress/strain rate perturbations triggered by an earthquake nearby followed by

450 postseismic slip and interseismic creep is an equally feasible mechanism to explain the deformation

451 sequence recorded in our sample. However, our preferred interpretation is that the transient brittle

452 deformation recorded in our studied sample is the manifestation of a slow slip event, for the following

453 reasons: (1) subduction interface SSEs typically occur at the downdip transition from stick-slip

454 behaviour to aseismic creep (e.g. Wallace and Beavan, 2010), and, in granitoid rocks, this transition is

455 expected to occur at the T range of deformation of our case-study, as witnessed by the deformation

456 microstructures of quartz and feldspar in the host protomylonite; (2) SSEs are often related to high pore

457 fluid pressure (e.g. Liu and Rice, 2007).

458 Whatever the actual process triggering brittle deformation was, we want to emphasize that detailed

459 microstructural studies of exhumed shear zones are a valuable complement to the geodetic,

460 seismological and experimental studies that aim to unravel the complex fault-slip behaviours at the

461 subduction interface. In this context, our studied sample represents a new and still not yet documented

462 case study of brittle-viscous transition zone and processes in subducted continental crust. Moreover, our

463 study reinforces the concept that the external zones of Alpine Corsica represent a unique target to

464 document and understand footwall deformation structures and processes related with HP/LT continental

465 subduction.

466

467 **8. References**

468

469

470 Altenberger, U., Prosser, G., Grande, A., Günter, C., and Langone, A.: A seismogenic zone in the deep
471 crust indicated by pseudotachylytes and ultramylonites in granulite-facies ricks of Calabria (Southern
472 Italy), Contributions to Mineralogy and Petrology, 166, 975-994, 2013.

473

474 Amitrano, D., and Schmittbuhl, J.: Fracture roughness and gouge distribution of a granite shear band,
475 Journal of Geophysical Research, 107, B12, doi:10.1029/2002JB001761, 2002.

476

477 Andersen, T.B., and Austrheim, H.: Fossil earthquakes recorded by pseudotachylytes in mantle
478 peridotites from the Alpine subduction complex of Corsica. Earth and Planetary Science Letters 242,
479 58-72, 2006

480

481 Andersen, T.B., Austrheim, H., Deseta, N., Silkoset, P., and Ashwal, L.D.: Large subduction
482 earthquakes along the fossil Moho in Alpine Corsica. Geology, 42, 395-398, 10.1130/G35345.1, 2014.

483

484 Angiboust, S., Glodny, J., Oncken, O., Chopin, C. In search of transient subduction interfaces in the
485 Dent Blanche–Sesia Tectonic System (W. Alps), Lithos, 205, 298-321, 2014.

486

487 Angiboust, S., Kirsch, J., Oncken, O., Glodny, J., Monié, P., and Rybacki, E.: Probing the transition
488 between seismically coupled and decoupled segments along an ancient subduction interface.
489 Geochemistry Geophysics Geosystems, 16, 1905-1922, doi:10.1002/2015GC005776, 2015.

490

491 Atkinson, B.K.: Subcritical crack propagation in rocks: theory, experimental result and applications.
492 Journal of Structural Geology, 4: 41–56, 1982.

493

494 Austrheim, H.: Fluid and deformation induced metamorphic processes around Moho beneath continent
495 collision zones: Examples from the exposed root zone of the Caledonian mountain belt, W-Norway,
496 Tectonophysics, 609, 620-635, 2013.

497

498 Austrheim, H. and Andersen T.B.: Pseudotachylytes from Corsica: fossil earthquakes from a subduction
499 complex. Terra Nova, 16, 193-197, 2004.

500

501 Austrheim, H., and Boundy, T.M.: Pseudotachylytes generated during seismic faulting and
502 eclogitization of the deep crust: Science, 265: 82-83, 1994.

503

504 Bedford, J., Moreno, M., Baez, J.C., Lange, D., Tilmann, F., Rosenau, M., Heibach, O., Oncken, O.,
505 Bartsch, M., Rietbrock, A., Tassara, A., Bevis, M., and Vigny, C.,: A high-resolution, time-variable
506 afterslip model for the 2010 Maule Mw 8.8, Chile megathrust earthquake, Earth Planet. Sci. Lett., 383,
507 26–36, 2013.

508

509 Berger, A. and Bousquet, R.: Subduction-related metamorphism in the Alps: review of isotopic ages
510 based on petrology and their geodynamic consequences. Geological Society, London, Special
511 Publications, 298, 117-144, 2008.

512

513 Beroza, G.C. and Ide, S.:   Slow Earthquakes and Non-volcanic Tremor, Annual Review of Earth and
514 Planetary Sciences, 39, 271-296, 2011.

515

516 Bestmann, M, and Prior, D.J.: Intragranular dynamic recrystallization in naturally deformed calcite
517 marble: diffusion accommodated grain boundary sliding as a result of subgrain rotation
518 recrystallization, Journal of Structural Geology, 25, 1597-1613, 2003.
519
520 Bezert, P., Caby, R.: Sur l'age post-bartonien des événements tectono-métamorphiques alpines en
521 bourdure orientale de la Corse cristalline. Bulletin de la Société Géologique de France, 8, 965–971,
522 1988.
523
524 Bos, B., Spiers, C.J.: Frictional-viscous flow of phyllosilicate-bearung rocks: Microphysical model and
525 implications for crustal strength profiles. Journal of Geophysical Research, 107, doi:
526 10.1029/2001JB000301, 2002.
527
528 Burg, J.P, Laurent, P.: Strain analysis of a shear zone in a granodiorite. Tectonophysics 47:15-42.
529 doi:10.1016/0040-1951 (78)90149-X, 1978.
530
531 Butler, R.H.W.: Area balancing as a test of models for the deep structure of mountain belts, with
532 specific reference to the Alps. Journal of Structural Geology 52, 2-16, 2013.
533
534 Carminati, E., and Doglioni, C.: Alps vs. Apennines: The paradigm of a tectonically asymmetric Earth,
535 Earth-Science Reviews 112 67–96: 2012.
536
537 Chester, F.M.: Dynamic recrystallization in semi-brittle faults. Journal of Structural Geology 11, 847-
538 858, 1989.
539
540 Cooper, F. J., Platt, J. P., Platzman, E. S., Grove, M. J., and Seward, G.: Opposing shear senses in a
541 subdetachment mylonite zone: Implications for core complex mechanics. Tectonics, 29,
542 10.1029/2009TC002632, 2010.
543
544 Derez, T., Pennock, G., Drury, M., and Sintubin, M.: Low-temperature intracrystalline deformation
545 microstructures in quartz. Journal of Structural Geology, 71, 3-23, 2015.
546
547 Deseta, N., Andersen, T.B., and Ashwal, L.D.: A weakening mechanism for intermediate depth
548 seismicity? Detailed petrographic and microstructural observation from blueschist facies
549 pseudotachylytes, Cape Corse, Corsica. Tectonophysics 610, 138-149, 2014a
550
551 Deseta, N., Ashwal, L.D., and Andersen, T.B.: Initiating intermediate-depth earthquakes: Insights from
552 a HP-LT ophiolite from Corsica. Lithos, 206, 127-146, 2014b.
553
554 Di Rosa, M., De Giorgi, A., Marroni, M. and Vidal., O. Syn-convergent exhumation of continental
555 crust: evidence from structural and metamorphic analysis of the Monte Cecu area, Alpine Corsica
556 (Northern Corsica, France). Geological Journal, doi: 10.1002/gj.2857: 2016.
557
558 Di Vincenzo, G., Grande, A., Prosser, G., Cavazza, W., and De Celles, P.G.: 40Ar–39Ar laser dating of
559 ductile shear zones from central Corsica (France): evidence of Alpine (middle to late Eocene) syn-burial
560 shearing in Variscan granitoids, Lithos, doi: 10.1016/j.lithos.2016.07.022, 2016.
561
562 Evans, B.W.: Phase relations of epidote-blueschists. Lithos 25, 3–23, 1990.
563
564 Faccenna, C., Piromallo, C., Crespo-Blanc, A., Jolivet, L., and Rossetti, F.: Lateral slab deformation
565 and the origin of the western Mediterranean arcs. Tectonics 23, TC1012, 2004.
566

Fagereng, Å, Hillary, G.W.B., and Diener, J.F.A.: Brittle-viscous deformation, slow slip, and tremor, Geophysical Research Letters, 41, 4159–4167, doi:10.1002/2014GL060433, 2014.

Fitz Gerald, J.D., and Stunitz, H.: Deformation of granitoids at low metamorphic grades. I. Reactions and grain size reduction. Tectonophysics 221, 269–297, 1993.

Fu, Y., and Freymueller, J.T.: Repeated large slow slip events at the south central Alaska subduction zone, Earth Planet. Sci. Lett., 375, 303–311, 2013.

Fusseis, F., and Handy, M.R.: Micromechanisms of shear zone propagation at the brittle–viscous transition. Journal of Structural Geology 30, 1242–1253, 2008.

Gapais, D., Bale, P., Choukroune, P., Cobbold, P.R., Mahjoub, Y., and Marquer, D.: Bulk kinematics from shear zone patterns: some field examples, Journal of Structural Geology, 9: 635-646. doi:10.1016/0191-8141(87) 90148-9, 1987.

Garfagnoli, F., Menna, F., Pandeli, E., and Principi, G.: Alpine metamorphic and tectonic evolution of the Inzecca-Ghisoni area (southern Alpine Corsica, France). Geological Journal, 44, 191–210, 2009.

Gibbons, W., and Horak, J.: Alpine metamorphism of Hercynian hornblende granodiorite beneath the blueschist facies schistes lustre´s nappe of NE Corsica. Journal of Metamorphic Geology 2, 95-113, 1984.

Golcalves, P-. Poilvet, J-C., Oliot, E., Trap, P., Marquer, D.: How does shear zone nucleate? An example from the Suretta nappe (Swiss Eastern Alps). Journal of Structural Geology 86, 166-180, 2016.

Guermani, A., and Pennacchioni, G: Brittle precursors of plastic deformation in a granite: An example from the Mont Blanc Massif (Helvetic, western Alps), Journal of Structural Geology, 20, 135–148, 1998.

Gueydan, F., Brun, J.P., Philippon, M., and Noury, M.: Sequential extension as record of Corsica rotation during Apennines slab roll-back. Tectonophysics, doi: 10.1016/j.tecto.2016.12.028, 2016.

Hacker, B.R., Peacock, S.M., Abers, G.A., Holloway S.D. Subduction factory 2. Are intermediate - depth earthquakes in subducting slabs linked to metamorphic dehydration reactions? Journal of Geophysical Research, 108, doi:10.1029/2001JB001129, 2003.

Handy, M.R., and Stunitz, H.: Strain localization by fracturing and reaction-weakening - a mechanism for initiating exhumation of subcontinental mantle beneath rifted margins. In: De Meer S., Drury M.R., De Bresser J.H.P., Pennock GM (eds) Deformation mechanisms, rheology and tectonics: current status and future perspectives, 200. Geological Society of London Special Publication, 387–407, 2002.

Handy M.R., and Brun, J.P.: Seismicity, structure and strength of the continental lithosphere. Earth and Planetary Science Letters 223, 427– 441, 2004.

Handy M.R., Hirth, G., and Burgmann, R.: Continental fault structure and rheology from frictional-to-viscous transition downward. In Tectonic Faults: Agents of Change on a Dynamic Earth. Handy, M.R., Hirth, G. and Hovious, N eds. Dahlem Workshop Reports, MIT press, 139-181, 2007.

Hayman, N.W., and Lavier, L.L.: The geologic record of deep episodic tremor and slip, Geology, 42, 195–198, doi:10.1130/G34990.1, 2014.

Healy, D., Reddy, S.M., Timms, N.E., Gray, E.M., and Vitale Brovarone, A.: Trench parallel fast axes of seismic anisotropy due to fluid-filled cracks in subducting slabs. Earth and Planetary Science Letters 283, 75-86, 2009.

Hirth, G., and Tullis, J.: Dislocation creep regimes in quartz aggregates, Journal of Structural Geology, 14: 145–159, 1992

Hirth, G., Teyssier, C., and Dunlop, W.J.: An evaluation of quartzite flow laws based on comparisons between experimentally and naturally deformed rocks, International Journal of Earth Sciences, 90, 77-87, 2001.

John, T., Medvedev, S., Rüpke, L.H., Andersen, T.B., Podladchikov, Y.Y., and Austrheim, Å.: Generation of intermediate-depth earthquakes by self-localizing thermal runaway, Nature Geoscience, 2, 137-140, doi:10.1038/NGEO419, 2009.

Jolivet, L., Dubois, R., Fournier, M., Goffé, B., Michard, A., Jourdan, C.: Ductile extension in Alpine Corsica. Geology 18, 1007-1010, 1990.

Kjøll, H.J., Viola, G., Menegon, L., and Sørensen, B.E.: Brittle-viscous deformation of vein quartz under fluid-rich lower greenschist facies conditions. Solid Earth, 6, 681-699, 2015.

Kohlstedt, D.L., Evans, B., and Mackwell, S.J.: Strength of the lithosphere: Constraints imposed by laboratory experiments, Journal of Geophysical Research, 100, 17857-17602, 1995.

Kruhl, J.H.: Prism- and basal-plane parallel subgrain boundaries in quartz: a microstructural geothermobarometer, Journal of Metamorphic Geology, 14, 581-589, 1996.

Küster, M, and Stöckhert, B.: High differential stress and sublithostatic pore fluid pressure in the ductile regime — microstructural evidence for short-term post-seismic creep in the Sesia Zone, Western Alps, Tectonophysics, 303, 263-277, 1999.

Lamb, S.: Shear stresses on megathrusts: Implications for mountain building behind subduction zones, J. Geophys. Res., 111, B07401, doi:10.1029/2005JB003916, 2006.

Liu, Y., and Rice, J.R.: Spontaneous and triggered aseismic deformation transients in a subduction fault model, J. Geophys. Res., 112, B09404, doi:10.1029/2007JB004930, 2007.

Maggi, M., Rossetti, F., Corfu, F., Theye, T., Andersen, T.B.: Faccenna, C., Clinopyroxene-rutile phyllonites from the East Tenda Shear Zone (Alpine Corsica, France): pressure-temperature-time constraints to the Alpine reworking of Variscan Corsica. Journal of the Geological Society 169, 723-732, 2012.

Magott, R., Fabbri, O., Fournier, M.: Subduction zone intermediate-depth seismicity: Insights from the structural analysis of Alpine high-pressure ophiolite-hosted pseudotachylytes (Corsica, France). Journal of Structural Geology 87, 95-114, 2016.

Magott, R., Fabbri, O., Fournier, M.: Polyphase ductile/brittle deformation along a major tectonic boundary in an ophiolitic nappe, Alpine Corsica: Insights on subduction zone intermediate-depth asperities Journal of Structural Geology 87, 95-114, 2016.

669

670 Malatesta, C., Federico, L., Crispini, L., Capponi, G.,: Fluid-controlled deformation in blueschist-facies
671 conditions: plastic vs brittle behaviour in a brecciated mylonite (Voltri Massif, Western Alps, Italy)
672 Geological Magazine, doi:10.1017/S0016756816001163, 2017.

673

674 Malasoma, A., Marroni, M., Musumeci, G., Pandolfi, L.: High pressure mineral assemblage in granitic
675 rocks from continental units in Alpine Corsica, France. Geological Journal, 41, 49–59, 2006

676

677 Mancktelow, N.S.: How ductile are ductile shear zones? Geology, 34, 345-348, 2006

678

679 Mancktelow, N.S., and Pennacchioni, G.: The control of precursor brittle fracture and fluidrock
680 interaction on the development of single and paired ductile shear zones. Journal of Structural Geology,
681 4, 27, 645–661, 2005.

682

683 Massonne, H.J., and Szpurka, Z.: Thermodynamic properties of white micas on the basis of high-
684 pressure experiments in the systems K2OMgO-Al2O3-SiO2-H2O and K2O-FeO-Al2O3-SiO2-H2O.
685 Lithos 41, 229-250, 1997.

686

687 Mattauer, M., Faure, M. and Malavieille, J.: Transverse lineation and large scale structures related to
688 Alpine obduction in Corsica. Journal of Structural Geology, 3, 401- 409, 1981.

689

690 Mazzoli, S., Vitale, S., Del Monaco, G., Guerriero, G., Margottini, C., and Spizzichino, D.: 'Diffuse
691 faulting' in the Machu Pichu granitoid pluton, Eastern Cordillera, Perù. Journal of Structural Geology,
692 31, 1395- 1408, 2009.

693

694 Meneghini, F., Di Toro, G., Rowe, C. D., Moore, J. C., Tsutsumi, A., and Yamaguchi, A.: Record of
695 mega-earthquakes in subduction thrusts: The black fault rocks of Pasagshak Point (Kodiak Island,
696 Alaska), Geol. Soc. Am. Bull., 122(7–8), 1280–1297, 2010.

697

698 Menegon, L., and Pennacchioni, G.: Local shear zone pattern and bulk deformation in the Gran
699 Paradiso metagranite (NW Italian Alps), International Journal of Earth Sciences, 99, 1805-1825, 2010.

700

701 Menegon, L., Piazolo, S. and Pennacchioni, G.: The effect of Dauphiné twinning on plastic strain in
702 quartz, Contributions to Mineralogy and Petrology, 161, 635-652, 2011.

703

704 Menegon, L., Stünitz, H., Nasipuri, P., Heilbronner, R., and Svahnberg, H.: Transition from fracturing
705 to viscous ow in granulite facies perthitic feldspar (Lofoten, Norway), Journal of Structural Geology,
706 48, 95-112, 2013.

707

708 Molli, G., Malavieille, J.: Orogenic processes and the Alps/Apennines geodynamic evolution: insights
709 from Taiwan. Int J Earth Sci, 100: 1207-1224, doi: 10.1007/s00531-010-0598-y, 2011.

710

711 Molli., G., Malasoma, A., Meneghini, F.: Brittle precursors of HP/LT microscale shear zone: a case
712 study from Alpine Corsica. 15th Conference of Deformation, Rheology and Tectonics, Zurich, Abstract
713 Volume, 153, 2005.

714

715 Molli, G.: Localizzazione di zone di taglio HP/LT su precursori fragili: Un esempio dalla Corsica
716 Alpina, Rend. Soc. Geol. It., 4 Nuova Serie, 270-271, 2007.

717

718 Molli, G.: Northern Apennine-Corsica orogenic system: an updated review. In: Siegesmund, S.,
719 Fugenschuh, B., Froitzheim, N. (Eds.), Tectonic Aspects of the Alpine-Dinaride-Carpathian System.

720   Geological Society, London Special Publications, 298, 413- 442, 2008.

722   Molli, G., White, J.C., Kennedy, L., and Taini, V.: Low-temperature deformation of limestone, Isola
723   Palmaria, Northern Apennine, Italy - The role of primary textures, precursory veins and intracrystalline
724   deformation in localization. Journal of Structural Geology, 33, 255-270, doi: 10 .1016 /j .jsg .2010 .11
725   .015, 2011.

727   Neumann, B.: Texture development of recrystallised quartz polycrystals unravelled by orientation and
728   misorientation characteristics. Journal of Structural Geology, 22, 1695-1711, 2000.

730   Ozawa, S., Murakami, M., Kaidzu, M., Tada, T., Sagiya, T., Hatanaka, Y., Yarai, H., and Nishimura,
731   T.: Detection and monitoring of ongoing aseismic slip in the Tokai region, central Japan, Science,
732   298(5595), 1009–1012, 2002.

734   Passchier, C.W., and Trouw, R.A.J.: Microtectonics. Springer. 366p., 2011.

736   Pec, M, Stünitz, and Heilbronner, R.: Semi-brittle deformation of granitoid gouges in shear experiments
737   at elevated pressures and temperatures, Journal of Structural Geology, 38, 200-221, 2012.

739   Peng, Z., and Gomberg, J.: An integrated perspective of the continuum between earthquakes and slow
740   slip phenomena, Nature Geoscience, 3, 599–607, 2010.

742   Pennacchioni, G.: Control of the geometry of precursor brittle structures on the type of ductile shear
743   zone in the Adamello tonalites, Southern Alps (Italy), Journal of Structural Geology, 27, 627-644, 2005

745   Pennacchioni, G., and Mancktelow, N.S.: Nucleation and initial growth of a shear zone network within
746   compositionally and structurally heterogeneous granitoids under amphibolite facies conditions, Journal
747   of Structural Geology, 29, 1757-1780, 2007.

749   Pennacchioni, G., and Zucchi, E.: High temperature fracturing and ductile deformation during cooling
750   of a pluton: The Lake Edison granodiorite (Sierra Nevada batholith, California), Journal of Structural
751   Geology, 50, 54-81, 2013.

753   Pennacchioni, G., Di Toro, G., Brack, P., Menegon, L., and Villa, I.M.: Brittle–ductile–brittle
754   deformation during cooling of tonalite (Adamello, Southern Italian Alps), Tectonophysics 427, 171–
755   197, 2006.

757   Pittarello, L., Pennacchioni, G., and Di Toro, G.: Amphibolite-facies pseudotachylytes in Premosello
758   metagabbro and felsic mylonites (Ivrea Zone, Italy), Tectonophysics, 580, 43-57, 2012.

760   Platt, J.P., and Behr, W.M.: Lithospheric shear zones as constant stress experiments, Geology, 39, 127-
761   130, doi: 10.1130/G31561.1, 2011.

763   Polino, R., Dal Piaz, G.V., and Gosso, G.: Tectonic erosion at the Adria margin and accretionary
764   process for the Cretaceous orogeny of the Alps. In: Roure, F., Heitzman, P., and Polino, R. (eds) Deep
765   Structure of the Alps. Volume Speciale Società Geologica Italiana, Roma, 1, 345–367, 1990.

767   Prior, D.J., Wheeler, J., Peruzzo, L., Spiess, R., and Storey, G.: Some garnet microstructures: an
768   illustration of the potential of orientation maps and misorientation analysis in microstructural studies.
769   Journal of Structural Geology, 24, 999-1011, 2002.
770

Ramsay, J.G., and Graham, R.H.: Strain variation in shear belts. Canadian Journal Earth Science 7, 786–813, 1970.

Rosenberg, C., and Kissling, E.: Three-dimensional insight into Central-Alpine collision: Lower-plate or upper-plate indentation? Geology, 41, 1219-1222, doi:10.1130/G34584.1, 2013.

Rossi, P., Durand-Delga, M., Lahondére, J. C., and Lahondére, D.: Carte géologique de la France à 1/50.000, feuille Santo Pietro di Tenda, BRGM, 2003.

Rutter, E. H: On the nomenclature of mode of failure transitions in rocks, Tectonophysics, 122 (3-4), 381- 387. 1986.

Schiffman, P., and Day, H.W.: Petrologic methods for the study of Very Low-grade metabasites in Low-Grade metamorphism (eds M. Frey and D. Robinson), Blackwell Publishing Ltd., Oxford, UK: doi: 10.1002/9781444313345.ch4, 2009.

Schmid, S.M., and Handy, M.R.: Towards a genetic classification of fault rocks: Geological usage and tectonophysical implications, in Muller, D.W., et al., eds., Controversies in modern geology: London, Academic Press, 339–361. 1991.

Schmid, S. M., Pfiffer, O.A., Froitzheim, N., Schonborn, G. and Kissling, E., Geophysical-geological transect and tectonic evolution of the Swiss-Italian Alps. Tectonics, 12, 1036-1064: 1996.

Scholz, C.H.: The brittle-plastic transition and the depth of seismic faulting. Geologische Rundschau, 77, 319-328, 1988.

Scholz, C.H.: The Mechanics of Earthquakes and Faulting, 2nd ed., Cambridge University Press, 2002.

Segall, P., and Simpson, C.: Nucleation of ductile shear zones on dilatant fractures, Geology, 14, 56–59, 1986.

Shimamoto, T.: The origin of S-C mylonites and a new fault-zone model, Journal of Structural Geology 11, 51-64, 1989.

Shimamoto, T., Logan, J.M. Velocity-dependent behaviours of simulated halite shear zones: an analog for silicates. Am. Geophys. Mongr., 37, 49-63, 1986.

Sibson, R.H.: Fault rocks and fault mechanisms, Journal of the Geological Society of London, 133, 191-213, 1977.

Sibson, R.H: Transient discontinuities in ductile shear zones, Journal of Structural Geology, 2, 165–171, 1980.

Sibson, R.H.: Continental fault structure and the shallow earthquake source, Journal of the Geological Society of London, 140, 741-767, 1983.

Sibson, R.H.: A note on fault reactivation, Journal of Structural Geology 7, 751–754, 1985.

Simpson, C.: Deformation of granitic rocks across the brittle-ductile transition, Journal of Structural Geology 7: 503-511, 1985.

822
823
824 Simpson, C.: Fabric development in brittle-to-ductile shear zones, Pure and Applied Geophysics 124 (1-
825 2), 269–288, 1986.
826
827 Stipp, M., Stunitz, H., Heilbronner, R. and Schmid, S.M.: The eastern Tonale fault zone: a 'natural
828 laboratory' for crystal plastic deformation of quartz over a temperature range from 250 to 700 °C. J
829 Struct Geol, 24, 1861-1884, 2002.
830
831 Stipp, M., and Tullis, J.: The recrystallized grain size piezometer for quartz, Geophysical Research
832 Letters, 30, 21, 2088, doi:10.1029/2003GL018444, 2003.
833
834 Stöckhert, B.: Stress and deformation in subduction zones - insight from the record of exhumed
835 metamorphic rocks, in Geological Society of London Special Publication, S. de Meer, et al., Editors.:
836 London, 255-274, 2002.
837
838 Takagi, H., Goto,   K., Shigematsu, N. Ultramylonite bands derived from cataclasite and
839 pseudotachylyte in granites, northeast Japan., J Struct Geol, 22, 1325-1339, 2000.
840
841 Tödheide, K.: Water at high temperatures and pressures, in Water: A Comprehensive Treatise, vol. 1,
842 edited by F. Franks, chap. 13, pp. 463–514, Springer, New York, 1972.
843
844 Trepmann, C.A., Stockhert, B., Dorner, D., Moghadam, E.H., Kuster, M. and Roller, K.: Simulating
845 coseismic deformation of quartz in the middle crust and fabric evolution during postseismic stress
846 relaxation – an experimental study. Tectonophysics 442, 83–104, 2007.
847
848 Tribuzio, R., and Giacomini, F., Blueschist facies metamorphism of peralkaline rhyolites from the
849 Tenda crystalline massif (northern Corsica): evidence for involvement in the Alpine subduction event?
850 Journal of Metamorphic Geology 20, 513-526, 2002.
851
852 Van Daalen, M., Heilbronner, R., Kunze, K.: Orientation analysis of localized shear deformation in
853 quartz fibres at the brittle–ductile transition, Tectonophysics, 303, 83-107, 1999.
854
855 Vannucchi, P., Remitti, F., and Bettelli, G.: Geological record of fluid flow and seismogenesis along
856 an erosive subducting plate boundary, Nature. 451, 7179,699-703, 2008.
857
858 Vernooij, M. G., den Brok, B., and Kunze, K.: Development of crystallographic preferred orientations
859 by nucleation and growth of new grains in experimentally deformed quartz single crystals,
860 Tectonophysics, 427, 35–53, 2006a.
861
862 Vernooij, M.G.C., Kunze, K. and den Brok, B.: 'Brittle' shear zones in experimentally deformed quartz
863 single crystals. J Struct Geol 28: 1292–1306, 2006b
864
865 Viola, G., Mancktelow, N. S., and Miller, J. A.: Cyclic frictional– viscous slip oscillations along the
866 base of an advancing nappe complex: insights into brittle-ductile nappe emplacement mechanisms from
867 the Naukluft Nappe Complex, central Namibia, Tectonics, 25, TC3016, doi:10.1029/2005 tc 001939,
868 2006.
869
870 Vitale Brovarone, A., Beyssac, Ol., Malavieille, J., Molli, G., Beltrando, M., and Compagnoni, R.
871 Stacking and metamorphism of continuous segments of subducted lithosphere in a high-pressure wedge:

872   The example of Alpine Corsica (France). Earth-Science Reviews, 116, 35–56, 2013.
873
874   Wallace, L.M. and Beavan, J.: Diverse slow slip behavior at the Hikurangi subduction margin, New
875   Zealand, Journal of Geophysical Research, 115, B12402, doi:10.1029/2010JB007717, 2010.
876
877   White, J.C. and White, S.H.: Semi-brittle deformation within the Alpine fault zone, New Zealand. J
878   Struct Geol 5: 579-589, 1982
879
880   White, J.C.: Transient discontinuities revisited: Pseudotachylyte, plastic instability and the influence of
881   low pore fluid pressure on deformation processes in the mid-crust. J Struct Geol 18: 1471-1477, 1996.
882
883   Zibra, I., Kruhl, J.H., and Braga, R.: Late Palaeozoic deformation of post-Variscan lower crust: shear
884   zone widening due to strain localization during retrograde shearing, International Journal of Earth
885   Sciences, 99, 973-991, 2010.
886
887
888
889
890
891

892   **Figures list and caption**

893

894   Fig.1 a) Alpine Corsica within the Alps/Apennine framework. b) Tectonic map of north Corsica

895   showing the main tectonic units and the area of studied sample. 1,2) Corsican continental crust, mainly

896   Carboniferous-Permian granitoids, their host pre-Carboniferous basement and a Mesozoic to Eocene

897   cover: (1a) "authochtonous" Hercynian Corsica and (1b) greenschist/lower-blueschist external

898   continental units (Corte; Popolasca); 2) inner continental units: (2a) upper-blueschist units (Tenda

899   Massif; Centuri) and (2b) eclogite slices (Serra di Pigno-Farinole); 3) Schistes Lustres nappe

900   (undifferentiated); 4) Nappe Superiore i.e. upper non-metamorphic units (Balagne, Nebbio and

901   Macinaggio units); 6) Miocene sediments; c) Regional cross-section with indication of study sample

902   from Popolasca area.

903

904   Fig.2. Mesoscopic view of the analyzed sample: protomylonitic metagranite host with millimetre-scale

905   ultramylonite localized after brittle precursor. All observable deformation structures were developed

906   under HP/LT metamorphic conditions.

907

908   Fig.3. Microscopic views of host-rock showing Quartz microstructures typical of low temperature

909   plasticity: a) intracrystalline deformation (undulatory extinction, deformation lamellae, deformation

910   bands, localized extinction bands, LEBs) associated with recrystallization along intragranular conjugate

911   shear bands sets; b) brittle fracturing in domino-style of K-feldspar associated with K-feldspar

912   breakdown to albite, stilpnomelane and phengite; c) quartz deformation lamellae and intergranular

913   recrystallization by bulging; d) K-feldspar intergranular recrystallization and albite-neocrystallization,

914   recrystallization also observable along later cracks and microfractures (horizontal to sub-horizontal).

915

916   Fig.4 a) BSE image of the metamorphic mineral assemblage in the host granitoids of the studied

917   sample; Ab, albite; Amp, Na-amphibole; Kfs, K-feldspar; Phe, phengite; Qtz, quartz; b) composition of

918   sodic amphiboles, using the classification of Leake et al. (1997); c) estimated peak-metamorphic

919   pressure/temperature conditions for the studied sample (cross-hatched area) constrained by the

920   reactions indicated.

921

922   Fig.5 a) Microscopic view of millimetre-scale shear zone nucleated after brittle precursor, with

923   indication of the structural-compositional domains within the shear zone. Domain 1 relict domain of

924   cataclasite; Domain 2 phyllonite; Domain 3 ultramylonite; b) detail of the sharp shear-zone boundary

925   heritage of former host-fracture contact and ultramylonite to phyllonite transition within the microscale

926   shear zone are well observable; c) detail of domain 1, relict domain of cataclasite, mainly K-feldspar

927   dominated. Angular fragments of variable size are indicative of brittle comminution.

928

929   Fig. 6   Microscopic view of ultramylonite; a) synkinematic Na-amphibole, boudinaged within the

930   quartz and albite ultramylonite matrix; b) Quartz and albite recrystallized matrix, in the lower part the

931   boundary of microscale shear zone with an host quartz porphyroclast; c) Quartz-ribbon with a strong

932   elongation (1:15, X/Z ratio) defining a shape preferred orientation oblique (15°) to the shear zone

933   boundary; d) detail of quartz recrystallization in the ribbon porphyroclast and matrix.

934

935   Fig. 7. EBSD analysis of quartz in the host protomylonite. (a) Microstructure of the analysed site. The

936   white arrows indicate localized extinction bands that have been analysed with the boundary trace

937   analysis and misorientation profiles as shown in Figs. 7b-g. (b) Inverse Pole Figure Map with the

938   respect to the protomylonitic foliation in the host rock (vertical in the figure). Location of subset 1 and 2

939   and trace of misorientation profiles 1-3 are shown. (c) Pole figure of the host grain, colour coded per the

940   quartz inverse pole figure shown in (b). (d) Pole figure of recrystallized quartz in the intracrystalline

941   bands. The blue and red line indicates the average orientation of the trace of the intracrystalline bands

942   with a subset 1 and 2 orientation, respectively. (e) Boundary trace analysis of the localized extinction

943   band of subset 1. (f) Boundary trace analysis of the localized extinction band of subset 2. (g) Point-to-

944   point misorientation profiles. See (b) for location of the traces of the profiles. (h) Misorientation axis of

945   the host grain and of the recrystallized grains in sample coordinates.

946

947   Fig. 8. EBSD analysis of quartz in the ultramylonite. (a) Microstructure of the recrystallized quartz from

948   domain 3 in the ultramylonite. (b) Pole figure of recrystallized quartz grains from (a). Only grains from

949   recrystallized ribbons in the ultramylonite were analysed.

950

951   Fig.9. a) Brittle failure analysis for our studied sample, see text for assumptions and approximations.

952   For the differential stress range and the vertical stress considered, brittle failure requires

953   (sub)lithostathic fluid pressure ($0.96 < \lambda < 1$) whereas viscous deformation at the estimated depth range

954   (23-30 km) is only possible for pore fluid pressure ≤ 0.94; b) Rheological profile calculated for a fixed

955   strain rate of 10^{-12} s^{-2} (see text for calculation details) using the quartz flow law of Hirth et al. (2001).

956   Cycle of switching in deformation style and mechanisms is suggested for the anayzed sample in its

957   ambient depth-range. Frictional Byerlee envelope is calculated using an average friction coefficient of

958   0.7 for various pore fluid pressure ratio values (Fig.9a and text). Stress estimates based on recrystallized

959   quartz piezometry (grey shaded area) have been calculated following Stipp and Tullis, (2003).

960

961

962 Fig.10. a) Simplified view of the ancient subduction of the corsican continental crust, with indication

963 where the mechanical coupling is the highest (seismogenic zone) and lowest (stable slip). The white

964 rectangle corresponds to the inferred zone of the studied sample. The pink to red shading figured the

965 lower to higher blueschist- to eclogite-facies peak metamorphism in continental-derived crustal units;

966 b,c,d Multi-stage scenario for development of the association of granitic protomylonites and

967 ultramylonites from brittle precursors in the Popolasca area: a) General sketch showing the east-dipping

968 ancient alpine subduction of the corsican continental crust. b): Formation of crustal scale anastomosed

969 network of shear zones within the host granitic crust, active distributed deformation with aseismic

970 creep; c: Formation of brittle instabilities (stage 2) in the shear zone by seismic ruptures nucleated along

971 the subduction interface (1) or the core of granites (2) and having propagated across and beyond the

972 granitic mylonites, followed by post-seismic creep, with locatization of shear zone after brittle precursor

973 (stage 3); d) Formation of brittle instabilities by seismic tremors and slow-slip events followed by post-

974 seismic (post-tremors) creep.

975
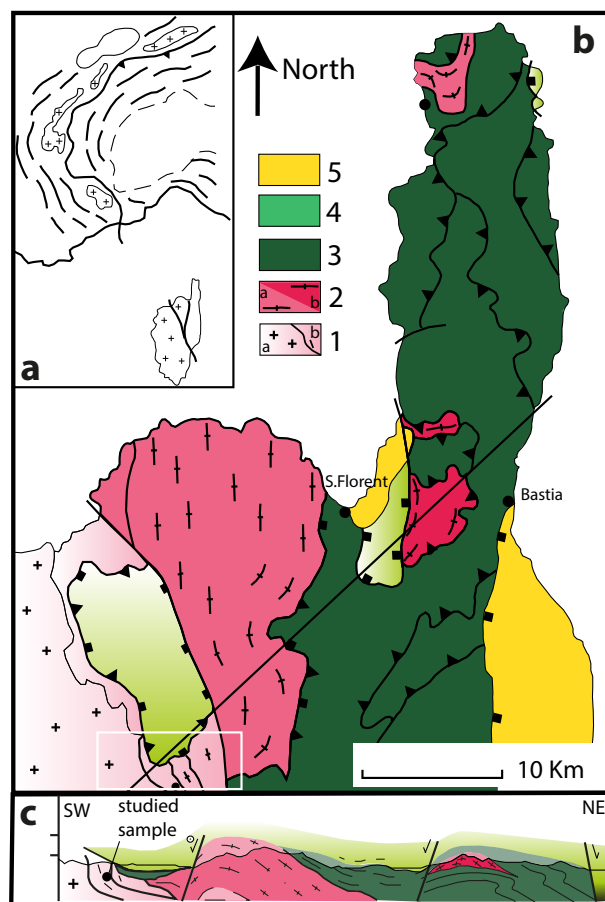
Fig.01
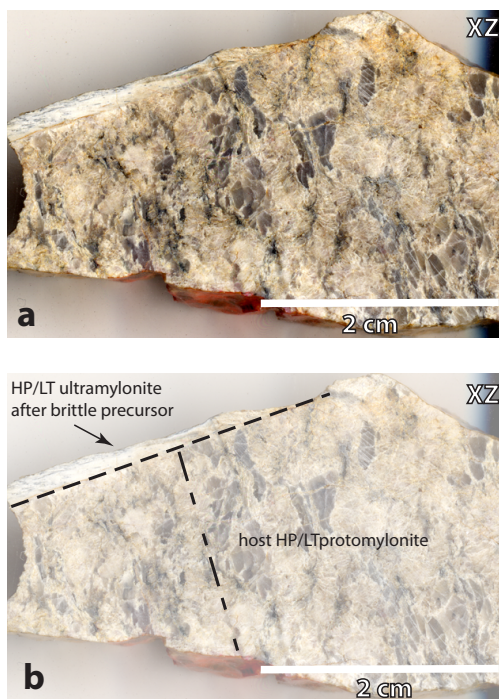
Fig.02
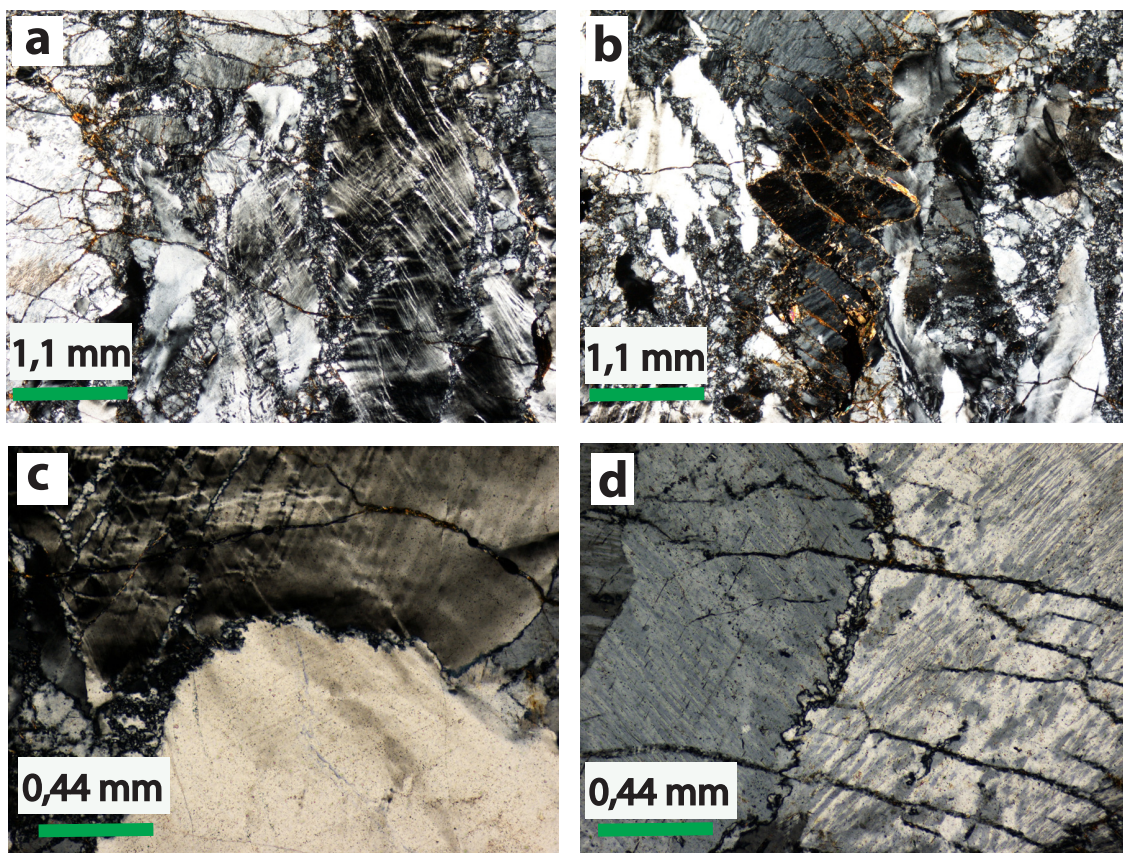
Fig.03
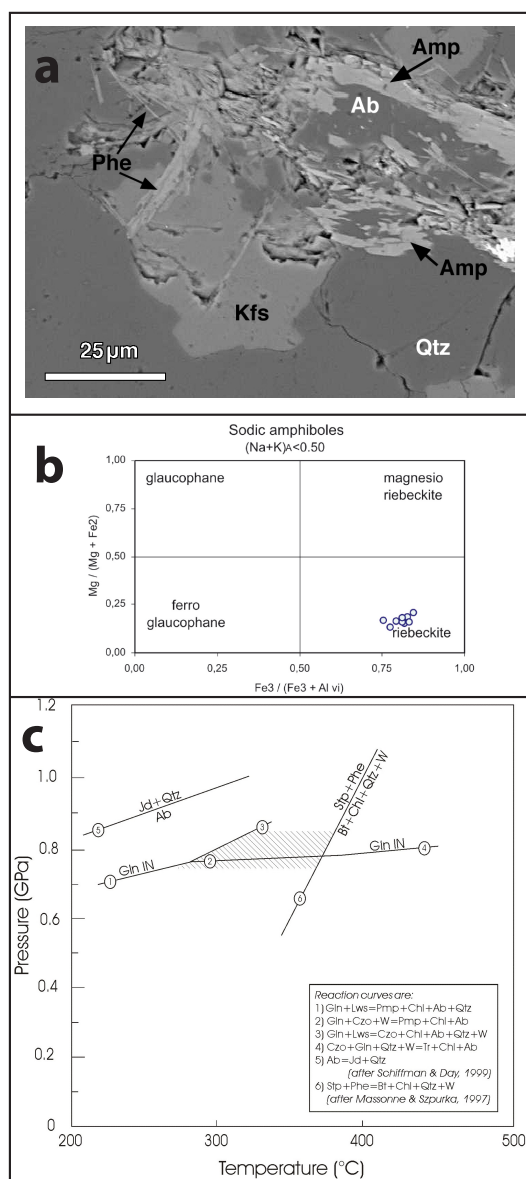
Fig.04
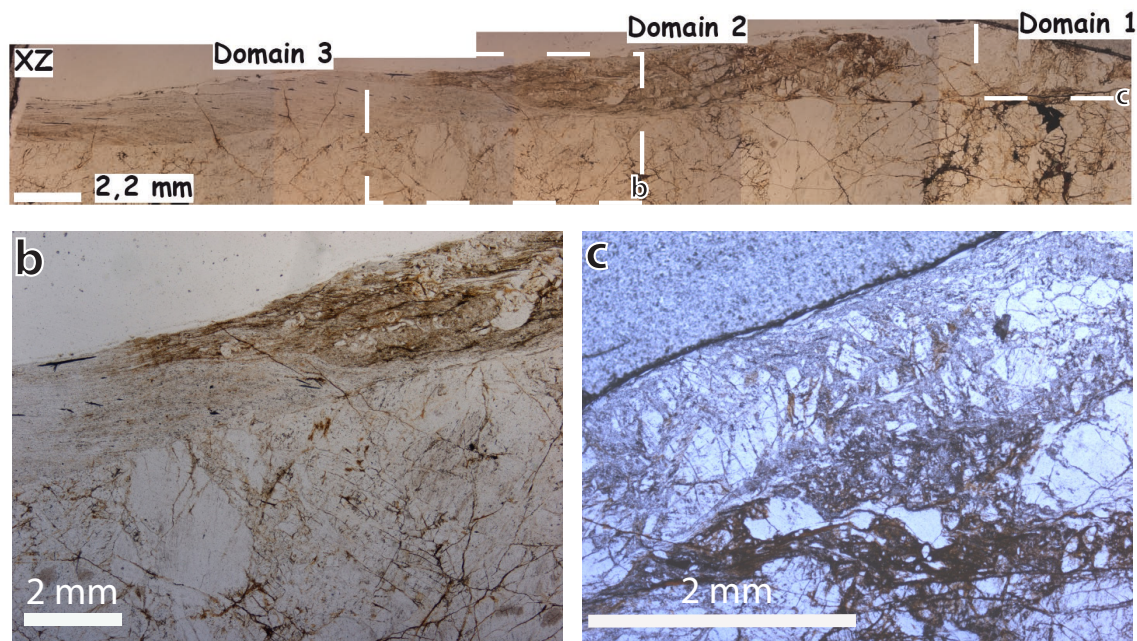
Fig.05

Fig.06

Fig.07

Fig.08
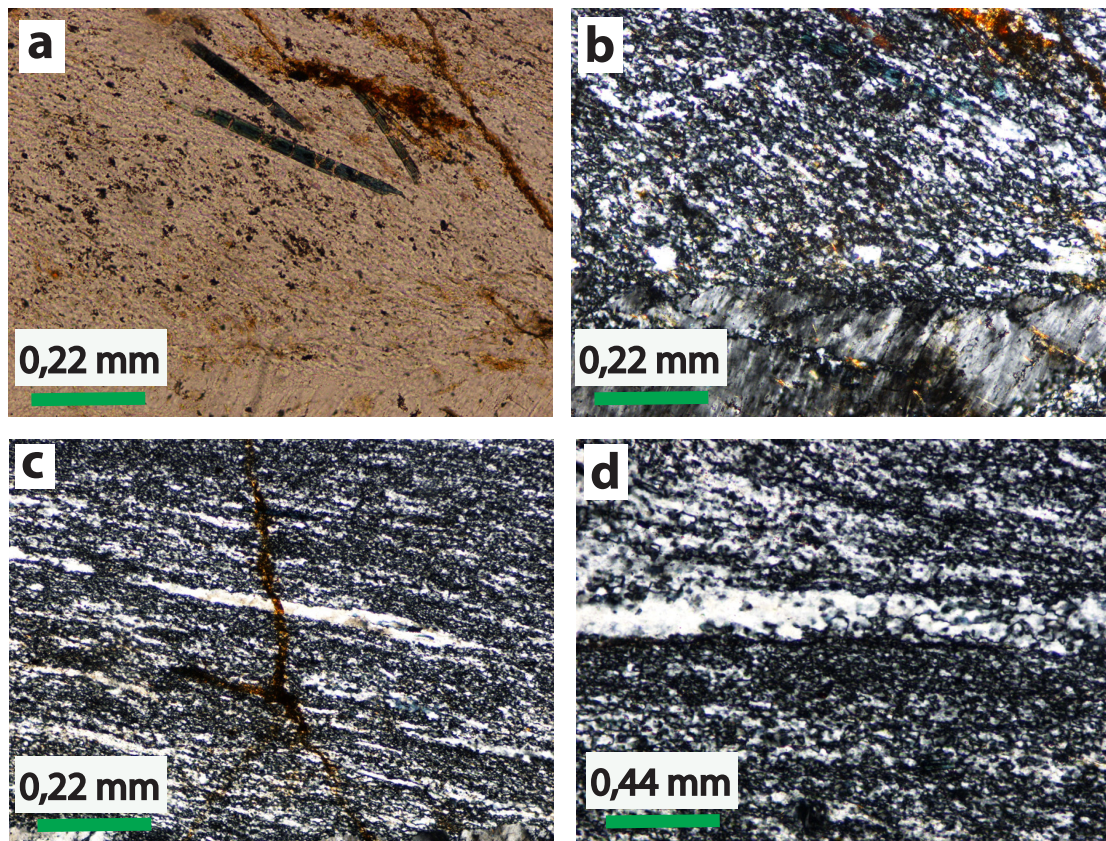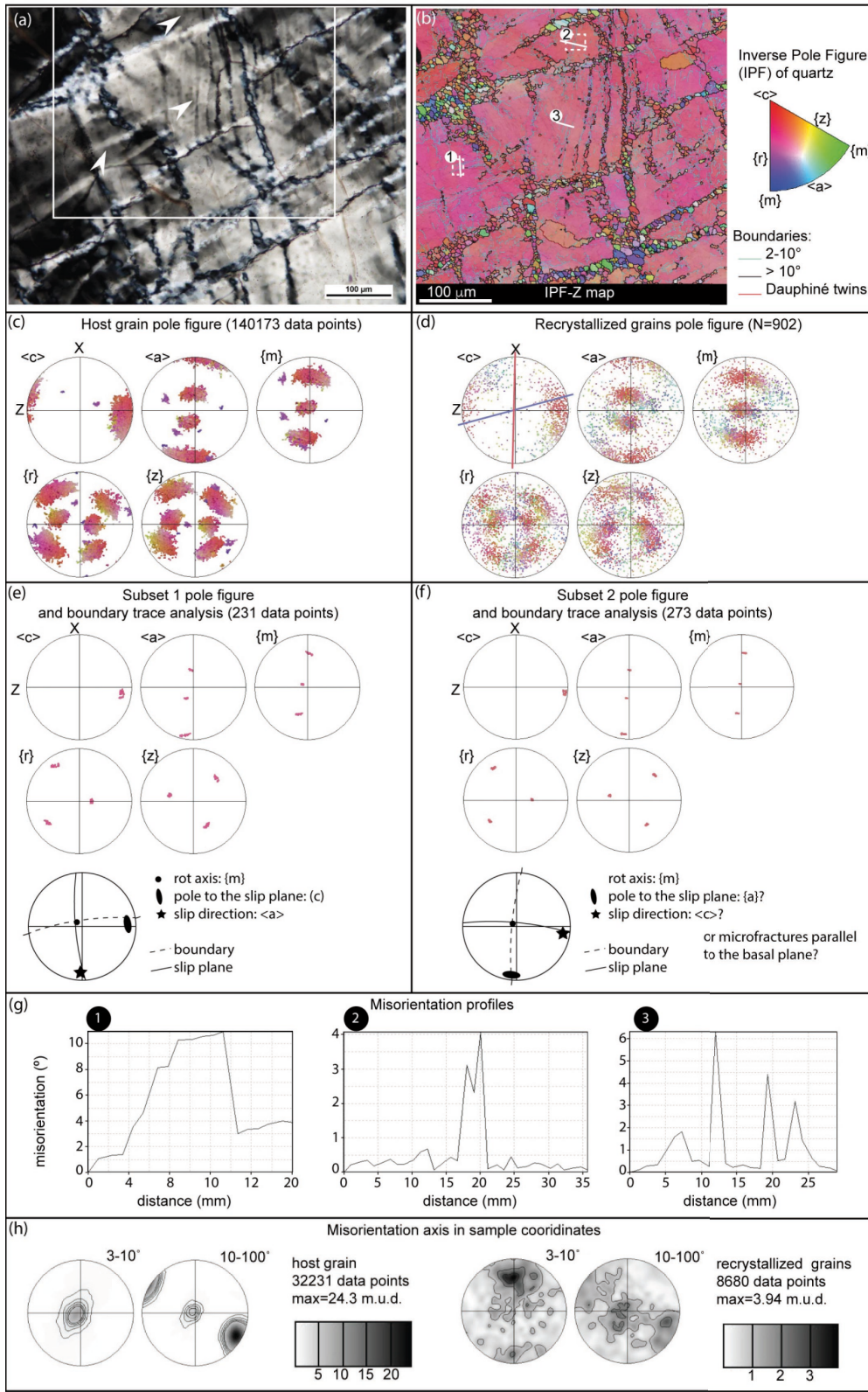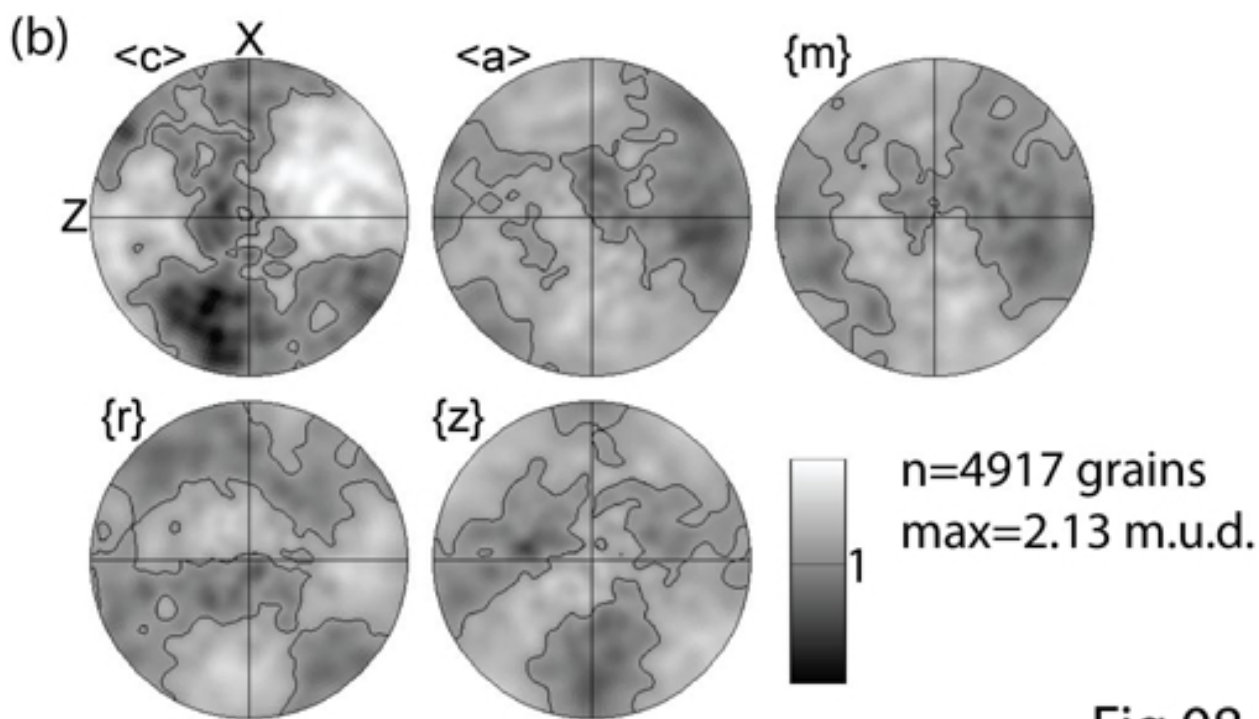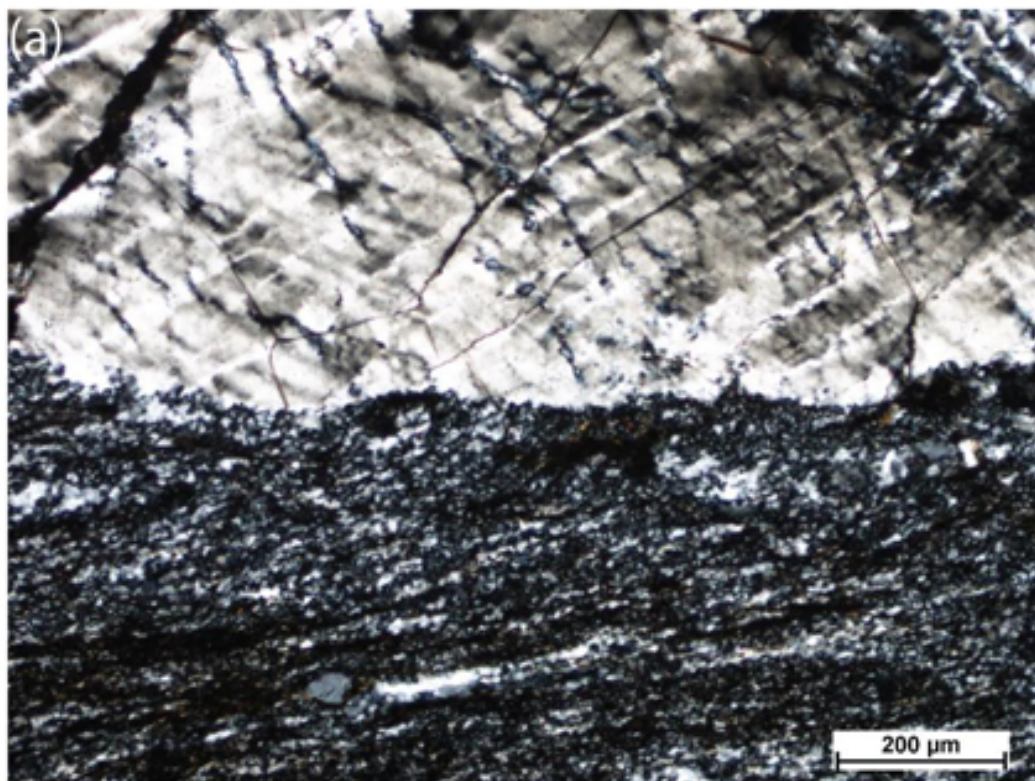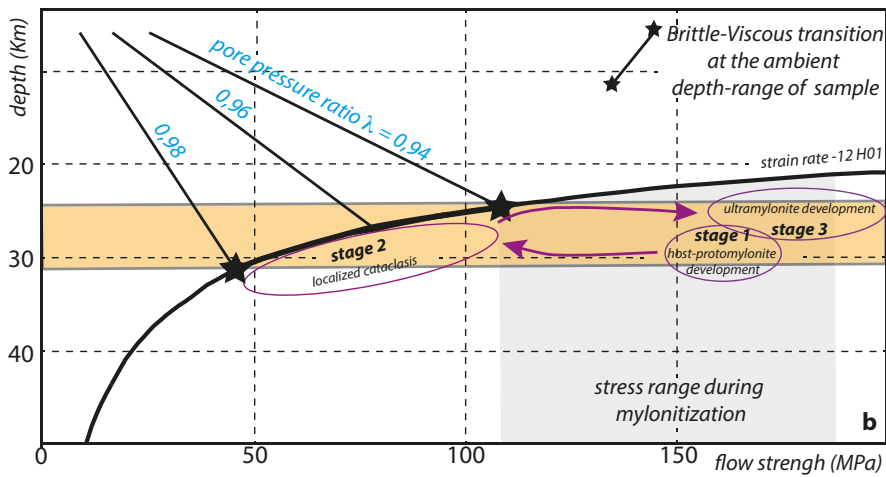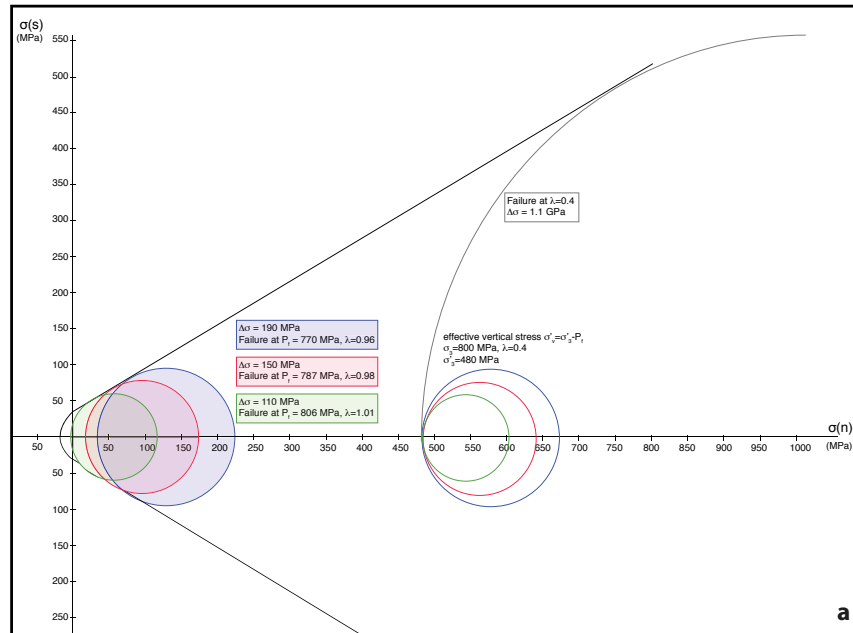
Fig.09
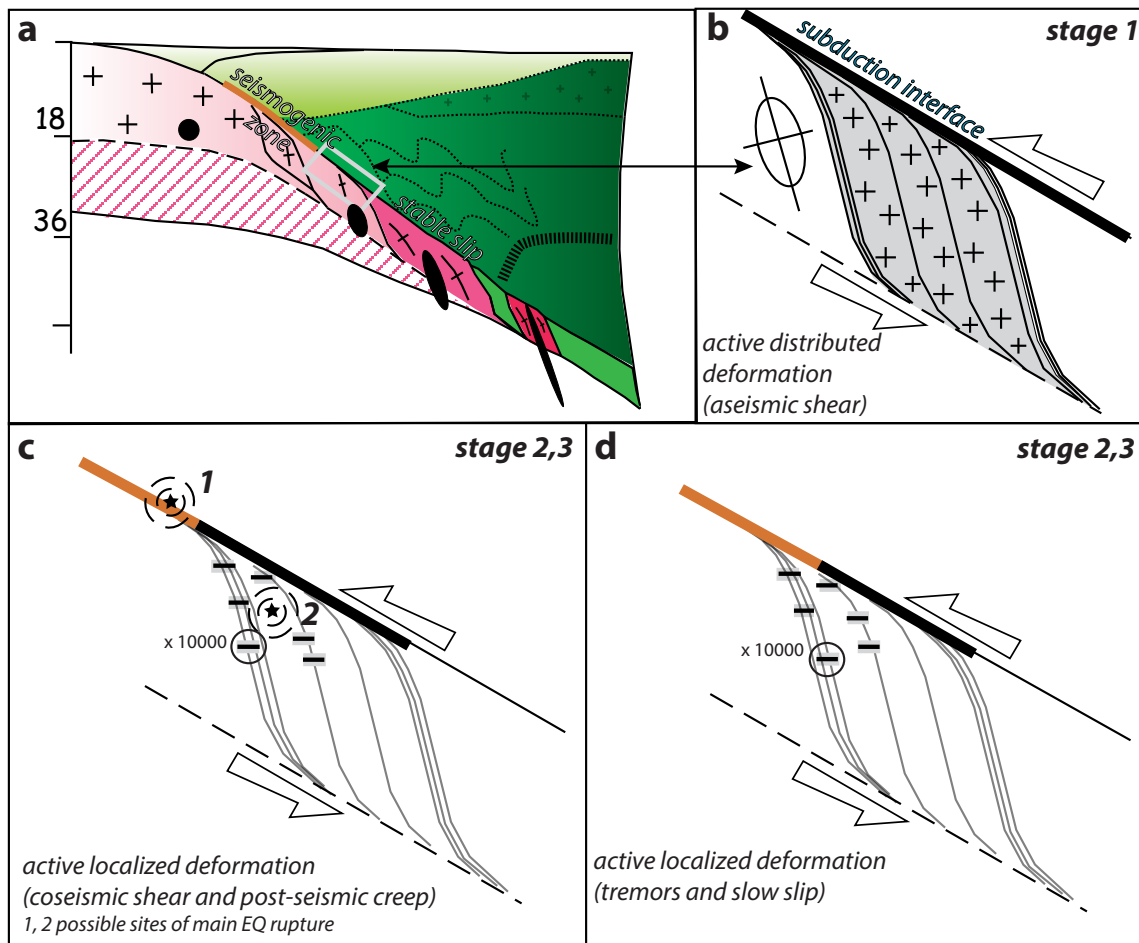
Fig.10

Amphibole	Am1	Am3	Am4	Am5	Am6N	Am6B	Am7
Wt%							
SiO2	51,58	51,30	50,62	50,97	50,28	50,61	52,62
TiO2	0,35	0,32	0,52	0,24	0,20	0,39	0,16
Al2O3	1,67	1,89	1,97	1,73	2,22	1,85	2,59
Cr2O3	0,00	0,00	0,00	0,00	0,00	0,00	0,00
FeO	28,13	29,65	28,80	28,77	30,25	30,18	27,94
MnO	0,00	0,15	0,00	0,20	0,00	0,00	0,00
MgO	2,24	1,86	1,97	2,16	1,64	1,98	1,90
CaO	0,06	0,05	0,10	0,09	0,13	0,14	0,06
Na2O	6,44	6,63	6,66	6,79	6,02	6,42	6,88
K2O	0,41	0,39	0,46	0,38	0,35	0,43	0,71
TOT	90,88	92,24	91,10	91,33	91,09	92,00	92,86
Cations							
Si	8,16	8,09	8,09	8,11	8,07	8,05	8,17
Al IV	0,00	0,00	0,00	0,00	0,00	0,00	0,00
Sum T	8,16	8,09	8,09	8,11	8,07	8,05	8,17
Al VI	0,31	0,35	0,37	0,32	0,42	0,35	0,47
Fe3+	1,70	1,56	1,42	1,54	1,46	1,50	1,45
Ti	0,04	0,04	0,06	0,03	0,02	0,05	0,02
Cr	0,00	0,00	0,00	0,00	0,00	0,00	0,00
Mg	0,53	0,44	0,47	0,51	0,39	0,47	0,44
Fe2+	2,02	2,35	2,43	2,28	2,61	2,51	2,18
Mn	0,00	0,02	0,00	0,03	0,00	0,00	0,00
Sum C	4,60	4,76	4,75	4,71	4,90	4,88	4,56
Mg	0,00	0,00	0,00	0,00	0,00	0,00	0,00
Mn	0,00	0,00	0,00	0,00	0,00	0,00	0,00
Fe2+	0,00	0,00	0,00	0,00	0,00	0,00	0,00
Ca	0,01	0,01	0,02	0,02	0,02	0,02	0,01
Na	1,97	1,99	1,98	1,98	1,87	1,98	1,99
Sum B	1,98	2,00	2,00	2,00	1,89	2,00	2,00
Na	0,00	0,04	0,08	0,11	0,00	0,00	0,08
K	0,08	0,08	0,09	0,08	0,07	0,09	0,14
Sum A	0,08	0,12	0,17	0,19	0,07	0,09	0,22
TOT	14,82	14,97	15,01	15,01	14,93	15,02	14,95

-: below detection limits

Stilpnomel:	Fill1	Fill2	Fill3	Fill4
Wt%				
SiO2	45,20	48,73	40,85	42,13
TiO2	0,13	0,07	0,30	0,18
Al2O3	21,19	12,22	17,08	20,28
Cr2O3	-	0,11	-	-
FeO	13,54	20,45	19,60	16,13
MnO	-	0,16	-	-
MgO	2,39	0,95	1,94	1,92
CaO	0,16	0,20	0,29	0,32
Na2O	0,16	1,00	0,37	0,26
K2O	4,68	3,00	5,05	4,89
TOT	87,45	86,89	85,48	86,11
Cations				
Si	7,418	8,292	7,235	7,200
Al vi	1,582	0,708	1,765	1,800
Sum Z	9,000	9,000	9,000	9,000
Al iv	2,516	1,743	1,800	2,284
Ti	0,016	0,009	0,040	0,023
Cr	0,000	0,015	0,000	0,000
Fe3+	0,000	0,000	0,000	0,000
Fe2+	1,858	2,909	2,902	2,304
Mn	0,000	0,023	0,000	0,000
	0,584	0,241	0,512	0,489
Sum Y	4,974	4,939	5,254	5,100
Ca	0,028	0,036	0,055	0,059
Na	0,051	0,330	0,127	0,086
K	0,979	0,651	1,141	1,066
Sum X	1,058	1,017	1,323	1,210
TOT	15,032	14,956	15,576	15,311

- : below detection limit

Feldspar	K-feld	K-feld	K-feld	K-feld	Albite	Albite	K-Feld	Albite	Albite	K-feld	Albite
Wt%											
SiO2	64,47	68,51	63,50	64,25	68,06	67,82	64,35	68,12	67,75	63,98	68,33
TiO2	-	-	-	-	-	-	0,02	-	-	-	0,07
Al2O3	18,75	20,33	18,32	18,66	20,50	19,84	18,28	19,43	20,20	18,91	20,43
Cr2O3	-	-	-	-	-	-	-	-	-	-	-
FeO	-	0,15	-	-	0,13	-	-	0,27	0,09	0,11	-
MnO	-	-	-	-	-	-	0,03	-	-	-	0,07
MgO	-	-	0,04	-	0,04	-	-	-	-	-	-
CaO	-	-	-	-	-	0,03	-	-	-	-	-
Na2O	2,44	0,18	0,17	0,19	11,03	11,44	-	11,31	11,56	0,20	11,17
K2O	13,48	9,05	16,32	14,72	0,28	0,05	15,74	0,16	0,04	14,39	0,56
TOT	99,14	98,22	98,35	97,82	100,04	99,18	98,42	99,29	99,64	97,59	100,63
Cations											
Si	11,92	12,25	11,95	12,02	11,88	11,93	12,03	11,99	11,88	11,98	11,88
Al	4,09	4,28	4,06	4,11	4,22	4,11	4,03	4,03	4,17	4,17	4,18
Sum Z	16,01	16,53	16,02	16,13	16,09	16,05	16,06	16,01	16,05	16,16	16,06
Fe3+	0,00	0,00	0,00	0,00	0,00	0,00	0,00	0,00	0,00	0,00	0,00
Fe2+	0,00	0,02	0,00	0,00	0,02	0,00	0,00	0,04	0,01	0,02	0,00
Mg	0,00	0,00	0,01	0,00	0,01	0,00	0,00	0,00	0,00	0,00	0,00
Ca	0,00	0,00	0,00	0,00	0,00	0,01	0,00	0,00	0,00	0,00	0,00
Na	0,87	0,06	0,06	0,07	3,73	3,90	0,00	3,86	3,93	0,07	3,76
K	3,18	2,06	3,92	3,51	0,06	0,01	3,75	0,04	0,01	3,44	0,12
Sum X	4,05	2,15	3,99	3,58	3,82	3,92	3,75	3,93	3,95	3,53	3,89
TOT	20,06	18,68	20,01	19,71	19,91	19,97	19,82	19,95	20,00	19,68	19,95
%Ab	21,58	2,93	1,56	1,92	98,36	99,57	0,00	99,08	99,77	2,07	96,81
%An	0,00	0,00	0,00	0,00	0,14	0,00	0,00	0,00	0,00	0,00	0,00
%Or	!"#$%	&!#'!	&"#$$	&"#'"	(#)$	'#%&	("#"	'#&%	'#%*	&!#&*	*#(&

tab 1